NMAMIT

NITTE

Annual Research Journal

Volume 4 October 2014 ISSN 2249-0426

STRIVE FOR EXCELLENCE
NMAMIT

Published by:
NMAM Institute of Technology
Nitte - 574 110
www.research.nitte.edu.in

EDITORIAL

The research at higher technical Institutions in India used to be the preserve of IITs. However, it is slowly and steadily entering the portals of tier 3 and lesser known institutions in the form of producing Ph.Ds. But, for the research to take firm hold in smaller Institutions, research beyond Ph.D must happen. For that, the departments must be staffed with number of faculty members more than the current AICTE requirement. That way there is less teaching/lab load on the faculty members and they can devout more time to research. I do foresee a scenario where in the faculty members are required to carry out research which has relevance to the societal problems, unlike just producing few research publications. Days are not too far off when the career advancement in higher technical Institutions will be mainly based on research related performance. It will not be wishful thinking if faculty members will be asked to generate income for themselves by way of carrying out consultancy for which they need to equip themselves well and be more relevant which is possible by carrying out research keeping in view the problems of the society. I am happy to note that couple of papers published in this journal respond to these requirements. I thank all the authors for their contribution. Happy and prosperous New Year 2015.

Dr. Sudesh Bekal
Editor

MEMBERS OF EDITORIAL BOARD

NMAMIT
Annual Research Journal

Volume 4
October 2014
ISSN 2249-0426

Published by:
NMAM Institute of Technology
An Autonomous Institution Under VTU, Belgaum
(A Unit of Nitte Education Trust)
NITTE - 574 110, UDUPI DIST., KARNATAKA
www.nitte.edu.in/nmamit

NMAMIT Annual Research Journal Volume No. 4

October 2014

ISSN : 2249-0426

Published by :

NMAM Institute of Technology

Nitte, 574 110

Udupi district, Karnataka State, India

Printed by :

Praveena Mudrana

Karkala 574104,

Udupi district, Karnataka State

email: praveenamudrana@gmail.com

A control strategy for a Positive Buck–Boost Converter using Buck and Boost Converter Combination

Jyothi [#1], Nayana P Shetty [#1]

[#] *Department of Electrical and Electronics, NMAMIT, Nitte, Karnataka, India*

[2] `nayanaps2002@yahoo.co.in`

Abstract— **A novel control strategy for improving the transients in the output voltage of a DC–DC positive buck–boost converter is presented in this paper. The proposed control technique can regulate the output voltage for variable input voltage, which is higher, lower, or equal to the output voltage. There are several existing solutions to these problems, and selecting the best approach involves a trade off among cost, efficiency, and output noise or ripple. The proposed method is unique of its kind from the point of view of improving the efficiency and ripple content in the output voltage.**

Keywords— **Control, efficiency, positive buck–boost converter, transients.**

I. INTRODUCTION

A very common power-handling problem, especially for portable applications, powered by batteries such as cellular phones, personal digital assistants (PDAs), wireless and digital subscriber line (DSL) modems, and digital cameras, is the need to provide a regulated non inverting output voltage from a variable input battery voltage. The battery voltage, when charged or discharged, can be greater than, equal to, or less than the output voltage. But for such small-scale applications, it is very important to regulate the output voltage of the converter with high precision and performance.

Thus, a tradeoff among cost, efficiency, and output transients should be considered. With an input voltage range that is above and below the output voltage, the use of a buck or a boost converter can be ruled out unless cascaded. Cascaded combination of converters results in cascaded losses and costs; therefore, this approach is seldom used. In such a range of power demand, the transition of DC voltage from one level to another is generally accomplished by means of Dc-Dc power converter circuits, such as step-down (buck) or step-up (boost) converter circuits.

In this paper, a novel theory is presented in order to fulfill the requirements of energy-efficient power supplies for battery- powered portable applications. The proposed method improves the transition problem and tries to reduce the transients happening during the transition from the buck mode to the boost mode.

II.TRANSITION PROBLEM

An example for a battery-powered application is shown in Fig.1.The input voltage of the battery when fully charged is 6 V and when discharged is 3.6 V. This supply needs to continuously provide a steady output of 5 V. Thus, the converter needs to operate in the buck mode for the period “T_A ,” followed by the buck–boost mode for “T_B ,” and finally in the boost mode for “T_C .”

The change in the duty ratio for different modes of operation based on different ranges of the input voltage is shown in Fig. 2. Referring to Fig. 1, for the period “T_A ,” the converter works in the buck mode, where the duty changes from the minimum value when the input is 6 V to the maximum when the input is approximately between 5.1 and 4.9 V, as shown in Fig. 2; for the time “T_B ,” the converter is in buck–boost mode; and, finally, for the period “T_C ,” it is working in the boost mode. The points “A” and “B” in Fig. 2 are in reference to those in Fig. 1.

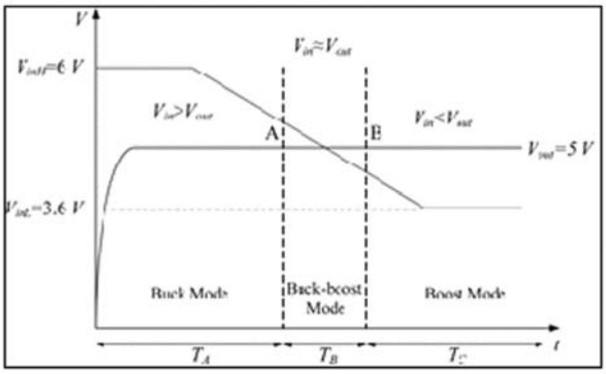

Fig. 1 Input–output curve for the power supply.

III. EXISTING SOLUTIONS

There are various topologies such as inverting buck–boost converters, single-ended primary inductance converters (SEPICs), Cuk converters, isolated buck–boost converters, and cascaded buck and boost converters, which can be implemented to maintain a constant output voltage from a variable input voltage. The important points of concern for such low-voltage-range power supplies are output ripple, efficiency, space, and the cost.

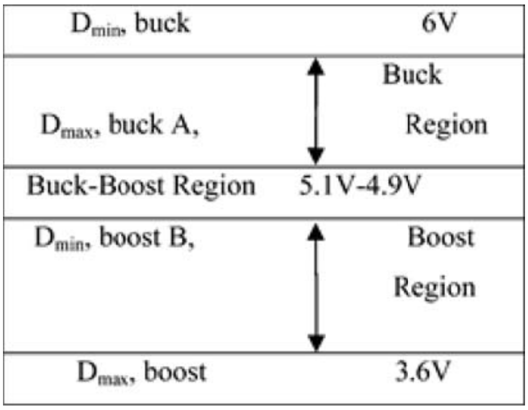

Fig. 2 Duty ratio variation for the buck and boost modes.

These topologies are generally not implemented for such power supplies due to their lower efficiency, higher size, and cost factors. The most difficult problem is the spikes in the output voltage, which causes the converter to lose efficiency during the transition from buck mode to the boost mode. Cost, size, switching speed, efficiency, and flexibility all need to be considered in designing such power supplies.

IV. PROPOSED METHOD

The proposed method is to add interface modes, which are a combination of buck and boost operating topologies (Figs. 3 and 4). As shown in Fig. 4, when the input voltage is considerably higher than V_1, the converter operates in purely buck mode. However, during the time period, where the input voltage is between V_1 and V_2, threshold voltage, the combination mode A comes into operation, followed by the buck–boost mode for the voltage range V_2 and V_3. In the voltage range V_3 and V_4, the converter operates in the combination mode B.

Finally, for the input voltages below V_4, the converter operates purely in the boost operating mode. By adding the combination modes A and B during the time periods "T_1" and "T_3" just before and after the stage, where $v_{\text{in}} \approx v_{\text{out}}$, the transient at the output of the converter can be improved significantly. Operation of the converter in buck– boost mode decreases the efficiency of the converter. In order to improve its efficiency, buck–boost mode should be eliminated. This is another major contribution of this paper. In that case, time periods T_2 will be eliminated and the operation mode will change from buck to the boost through intermediate combination modes.

Each combination mode is a combination of several buck and boost operating topologies. In the proposed method, instead of a sudden transition from buck operating mode to a buck–boost operating mode, a combination of buck and boost operating topologies is applied to distribute the voltage transient and, therefore, obtain smoother output waveform. This is the concept of digital combination of power converters (DCPCs), which is applied to a non-inverting buck–boost converter in this paper.

In combination mode A, the number of buck operating topologies is usually higher than the number of boost operations. Similarly, in the combination mode B, the number of boost operating modes will be higher than buck operations.

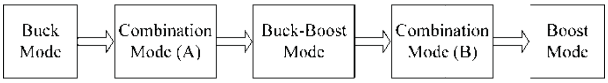

Fig.3 Combined-method-based control logic for deciding modes of operation.

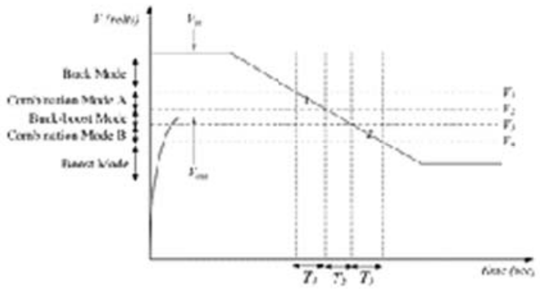

Fig.4 Voltage curves for combined-method-based control.

Operation of Positive Buck–Boost Converter

The circuit topology of a positive buck–boost converter is shown in Fig. 5. In buck–boost operating mode, always, two switches, Q_1 and Q_2, and two diodes, D_1 and D_2, are switching in the circuit. A positive buck–boost converter can operate as a buck converter by controlling switch Q_1 and diode D_1, when Q_2 is OFF and D_2 is conducting. It can also work as a boost converter by controlling switch Q_2 and diode D_2, while Q_1 is ON and D_1 is not conducting.

When the voltage of the battery is more than the output reference voltage, converter operates as a buck converter. As soon as the voltage of the battery drops to a value less than the output reference voltage, the converter should switch to boost mode. The added advantage of the converter is that the output of such a converter is always positive.

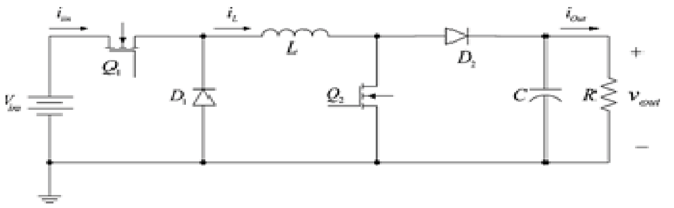

Fig. 5 Circuit topology of a positive buck–boost converter

The overall system level closed loop control strategy of the proposed method is shown in Fig. 6.

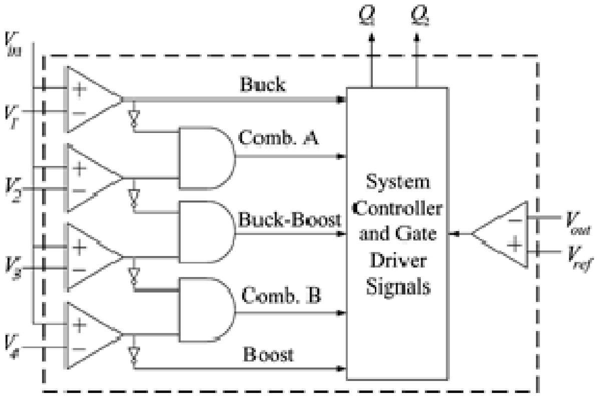

Fig 6: closed loop control strategy for the proposed method

V. SIMULATION RESULTS

The simulation results have been obtained for the converter based on the parameters shown in TableI.

TABLE I
PARAMETERS OF POSITIVE BUCK–BOOST CONVERTER

Variable	Parameter	Value
L	Magnetizing inductance	100µH
C	Output filter capacitance	330µF
Vin	Input voltage	6V-3.6V
Vref	Output voltage	5V
f	Switching frequency	100kHz
R	Output resistance	Value

1) Proposed Combination Method With Buck–Boost Mode in the Middle: The simulations were carried out on the converter using the buck–boost in the middle. This method improves the ripple content in the output voltage of the converter when the input voltage becomes almost equal to the output voltage and during other transition modes. The waveforms are shown in Fig.7. It is seen that the peak transient happening during the transition is about 4%.

2) Without Buck–Boost Mode in the Middle: The buck–boost mode, in the middle, was neglected to save the efficiency of the converter, since during this mode of operation, both the switches are operated simultaneously.

By applying this combination method of control and simulating the converter, the results shown in Fig.8 are obtained. This voltage variation in this method is about 4%; however, canceling the buck–boost operating mode in between significantly improves the efficiency of the converter. Fig.9 presents the output voltages for all different transition methods.

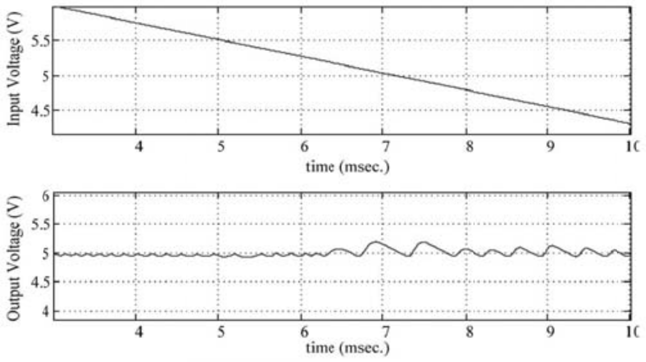

Fig.7 Input and output voltages for the transition from buck to boost through combination mode A, buck–boost, and combination mode A.

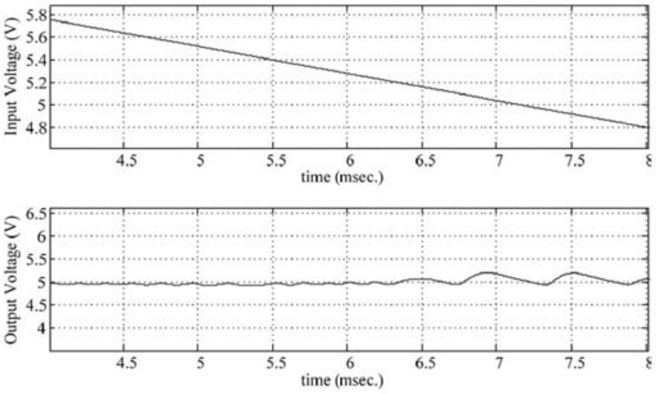

Fig.8 Input and output voltages and buck and boost pulses during transition from buck to combined mode A and then to combined mode B and boost without buck–boost mode.

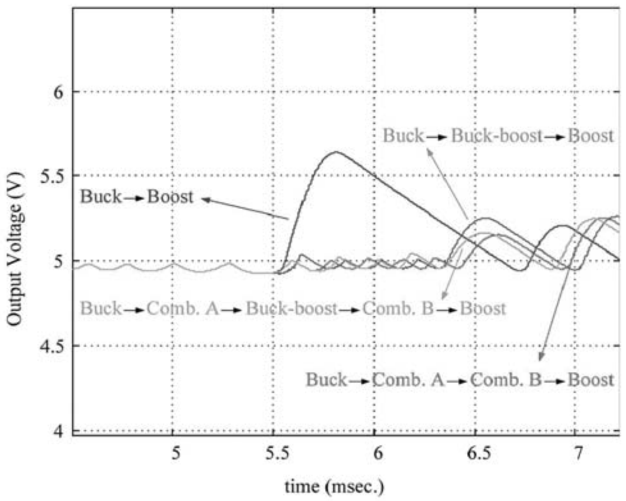

Fig.9 Output voltages for all four different transition methods

VI. EXPERIMENTAL SETUP

The hardware of a positive buck–boost converter is designed based on the parameters listed in Table I. The converter operates at 100 kHz switching frequency. Two n-type MOSFET switches and two Schottky barrier diodes are used for positive buck–boost converter configuration. The MOSFET switches and diodes are IRF540 and 1N5817, respectively. Controller has been implemented using a Texas Instrument digital signal processor (DSP) (320F2812). The output voltage reference is set to 5.0 V, and input voltage varies from 6.0 to 3.6 V.

Two high-side gate drivers are designed for IRF540. The dedicated gating logic is applied to the converter for proper operation as buck, buck–boost, and boost converters. The operating modes are dependent on mode selection signals, applied from DSP. The overall configuration of converter and controller is shown in Fig.10. G1 and G2 are buck pulse and boost pulse, sequentially. MD_SEL0, MD_SEL1, and MD_SEL2 determine operation modes: buck, combination mode A; buck–boost, combination mode B; and boost, in each control period.

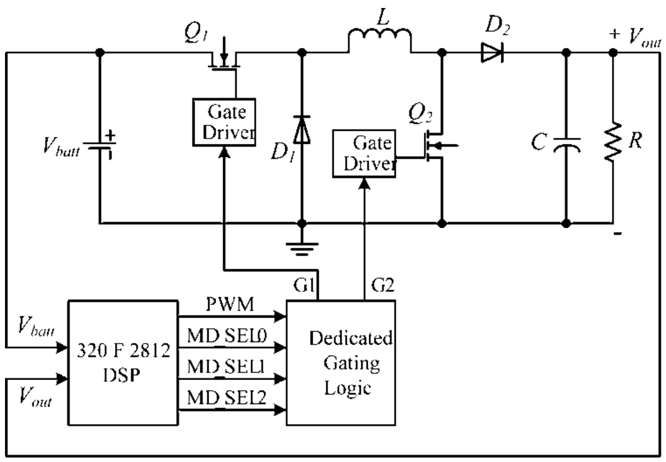

Fig.10 Experimental circuit configuration.

VII. CONCLUSIONS

A highly efficient control strategy to control a pulse width modulation (PWM) dc/dc positive buck–boost switching converter has been illustrated in this paper. The proposed control scheme can regulate the output voltage for an input voltage, which changes based on the charge status of the battery supply. In this method, the capability of skipping over higher loss interface stages such as buck–boost mode in the case of a positive buck–boost converter significantly improves the efficiency of the circuit topology.

ACKNOWLEDGMENT

My sincere thanks to our Head of the Dept., Prof. K Vasudev Shettigar, Dept. of E&EE, NMAMIT, Nitte for his support.

REFERENCES

[1] Young-Joo Lee, Alireza Khaligh, Arindam Chakraborty, and Ali Emadi, "Digital combination of buck and boost converters to control a positive buck–boost converter and improve the transients," IEEE transactions on Power Electronics, vol.24,No.5,May 2009.

[2] A. Chakraborty, A. Khaligh, A. Emadi, and A. Pfaelzer, "Digital combination of buck and boost converters to control a positive buck–boost converter," in *Proc. IEEE Power Electron. Spec. Conf.*, Jun. 2006, vol. 1, pp. 1–6.

[3] R. W. Erickson, *Fundamentals of Power Electronics*, 4th ed. Norwell, MA: Kluwer, 1999.

Corrosion Effects on Flexural Bond Strength of RC Members: An Experimental Investigation

Akshatha Shetty [#1], Katta Venkataramana[#2] and Babu Narayan K.S[#3].
[#]*Department of Civil Engineering, National Institute of Technology Karnataka, Surathkal-575025, Karnataka, India.*

[1] `akshathashetty16@gmail.com`

Abstract— **Bond is the interaction mechanism which enables the force transfer between surrounding concrete and steel. To evaluate the effect of corrosion on bond strength behavior National Bureau of Standard (NBS) beam specimen is considered for the study. Different corrosion levels such as 0%, 2.5%, 5% and 7.5% are considered. Impressed current technique is used to accelerate the corrosion process. Corrosion effects on load v/s strain and bond strength relations are studied. From the results it is observed that strain value of corroded beams is more compared to the controlled beam specimen for the applied load level. Increase in corrosion level causes degradation of the bond behavior.**

Keywords— **Corrosion, bond strength, load, strain, concrete**

I. INTRODUCTION

Chloride ingress in to the concrete is one of the primary causes of reinforcement corrosion. Once chloride comes in contact with the rebar level, passive layer present over the steel surface disappears and corrosion process initiates

The rust produced as a result of corrosion has a volume 2 to 6 times than that of original steel; it causes volume expansion developing tensile stresses in concrete [1]. Its effects on RC structures include cracking and spalling of the concrete cover, reduction, and eventually loss of bond between concrete and corroding reinforcement, and reduction of cross-sectional area of reinforcing steel. Corrosion affects both strength and serviceability of RC structures.

Composte action between concrete and reinforcing steel cannot occur without bond. One of the most important prerequisites of reinforced concrete construction is an adequate bond between the reinforcement and the concrete.

In the present study effect of corrosion on bond strength of PPC RC members is investigated.

II. EXPERIMENTAL INVESTIGATION

Preparation of Test Specimen

For the present study National Bureau of Standard (NBS) beam specimens of size 2.44mx0.457mx0.203m (Fig.1) are used. Beam specimen considered for the study is a under reinforced section. Concrete mix of M30 Grade is prepared using Portland Pozzolona cement concrete (PPC), fine sand and aggregate (20mm & 12.5mm size) as per IS 10262:2009[2]. Mix proportion of 1: 1.77: 2.87 is used for the present study. Water cement ratio of 0.45, with an addition of 2ml/kg of a commercially available chemical admixture is used to get desired slump. The slump obtained is 52mm. Compressive strength of 32.57N/mm^2 is achieved at the end of 2days.

After curing, beam specimens are subjected to desired corrosion levels. Electrochemical corrosion technique is used to accelerate the corrosion of steel bars embedded in beam specimens. Specimens are partially immersed in a 5% NaCl solution for a duration of 8 days. Eq (1) gives the amount of current to be applied to get desired levels of corrosion [3].

$$i_{app} = \frac{(\rho \times W_i \times F)}{100 \times \pi \times D \times L \times W \times T} \qquad (1)$$

where; $\rho =$ Degree of corrosion in percentage, T= Time in seconds, W_i= Initial weight of steel 20,000 in grams; F=96487 Amp-sec; W= Equivalent weight of steel (27.925grams), i_{app} = Applied current, D= diameter of bar, L=Length of ba.

Based on Eq.1, the amount of applied current was varied from 2.5A to 7.5A current at 2.5A increments, to achieve corrosion levels varying from 2.5%, to 7.5% at 2.5% increments. Detailed representation of accelerated corrosion process is shown in Fig. 2.

Corrosion Rate Measurement

Corrosion levels are measured with applied corrosion monitoring instrument (Fig. 3) based on linear polarization resistance (LPR) method to assure the desired degree of corrosion levels in beam specimens after inducing corrosion for a particular duration. Corrosion current densities are calculated for each specimen for different grids and average value is considered to calculate the weight loss (%) from Eq. 1. Corrosion current density is calculated by using the Stern-Geary formula

$$i_{corr} = \frac{B}{R_p} \tag{2}$$

where, i_{corr} = corrosion current density (μA/cm^2); R_p = polarization resistance (kΩ cm^2); B = 26 mV (for steel in active condition this value is normally used [4]).

Test Setup used for Flexural Bond tudy

Beam specimens are tested under two point loading condition. The load is applied at 15kN increments. Proving ring of 500kN capacity is used to note the applied load.

Strain value recordings have been done by using demec gauges at every load interval. Test setup with positions of Demec targets have been shown in Fig. 4.

Determination of Bond Stress

Average bond stress values are obtained from Eq. (3).

$$\tau_{bd} = \frac{\phi_1 \times f_s}{4 \times l_d} \tag{3}$$

where,

τ_{bd} = Average bond stress (N/mm^2)

l_d = Embedment length of the bar (747mm) from the test setup

f_s = Steel stress values

ϕ_1 = Reduced Diameter (mm) values

Reduced diameter can be obtained [5] from Eq. (4),

$$\phi_1 = \phi\sqrt{(1 - \frac{p}{100})} \tag{4}$$

where,

ϕ_1 = Reduced Diameter (mm)

ϕ = Initial Diameter (25mm)

p = Weight loss in percentage

The steel stress values have been obtained for initiation and end strain value at slip region for different corrosion levels from stress corresponding to strains at that load level (Fig. 5).

III. RESULTS AND DISCUSSION

Fig. 6 shows result of variation of corrosion levels with the icrease in the applied current. It is seen that corrosion levels increases linearly with the increase in the applied current.

From Fig. 7 it is seen that as the load level increases strain value increases linearly in the initial stage. Then at higher corrosion levels, rate of increase of strain is higher for the same increment of load level compared to lower level of corrosion. Control beam specimen performs better at increased corrosion levels. It is also observed that there is a sudden increase in strain values observed for the applied load interval, in all beam specimens. This indicates there is a slip between reinforcement and surrounding concrete; since the corresponding strain value for yield strength of 25mm diameter bar is much higher than the value of sudden increase in strain value. Slip at initiation indicates the point where flat portion begins and slip at end point where flat portion ends and strain values start continuing again.

Bar stress and Bond Stress performance of NBS beam

Bond stress results for different levels of corrosions ar obtained from Eq. (3). Percentage reduction in bond stress for different levels of corrosion i.e. 2.5%, 5%, and 7.5% with respect to control beam specimen are 4.32%, 10.65%, and 18.93% respectively.

From Fig. 8 it is observed that bond stress drops by about 2.1% (at initiation of slip) and 2.2% (at end of slip point) or every percentage increase in corrosion leve.

.

Bond stress values for different degree of corrosion can be calculated from following equations obtained from Fig.8, where x=corrosion level (%) and y= bond stress(N/mm^2).

At initiation of slip point:

$$y = -0.043x + 1.708 \qquad R^2 = 0.976 \tag{5}$$

At end of slip point

$$y = -0.018x + 3.262 \qquad R^2 = 0.983 \tag{6}$$

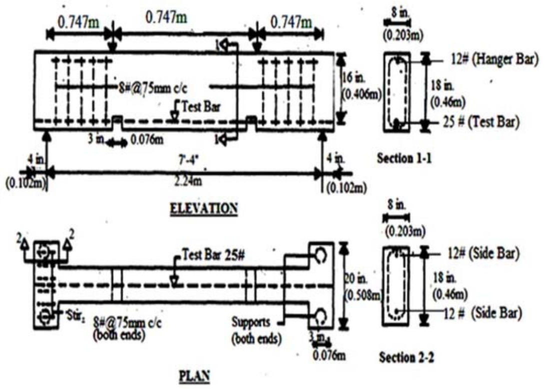

Fig. 1 Reinforcement details of NBS beam specimens

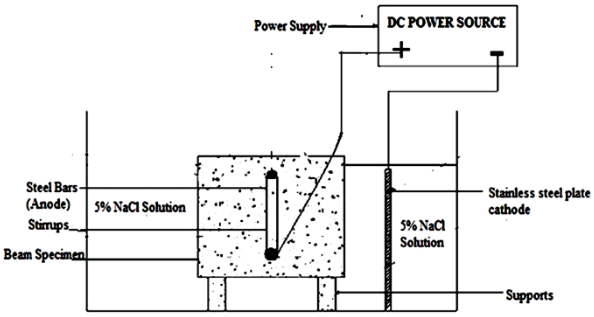

Fig. 2 Schematic representation of accelerated corrosion process

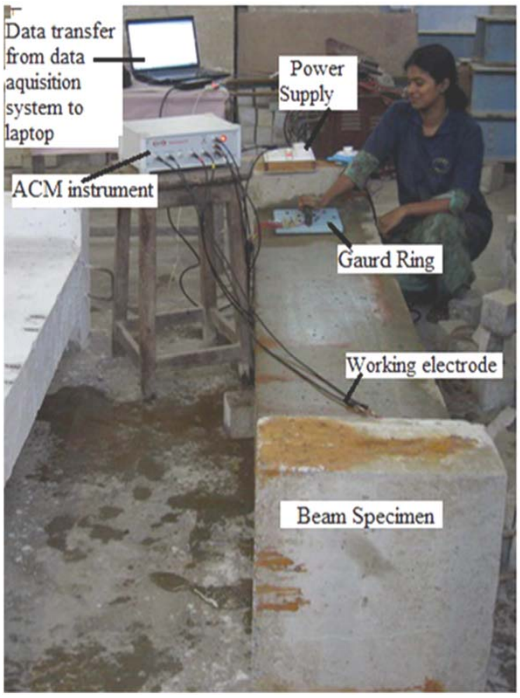

Fig. 3 Corrosion monitoring test setup

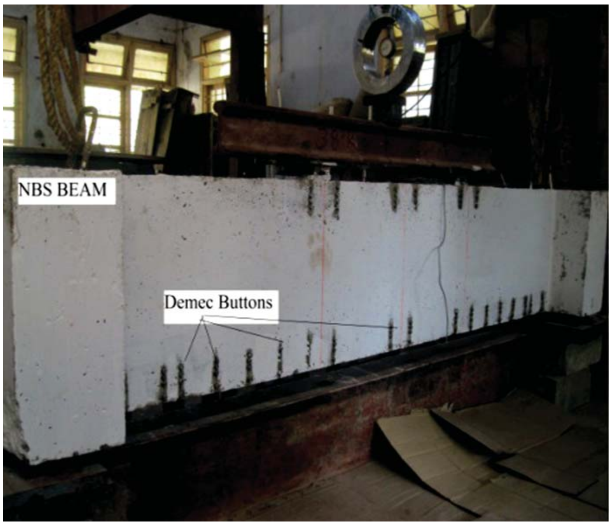

Fig. 4 Test set up used for the determination of Bond-strength

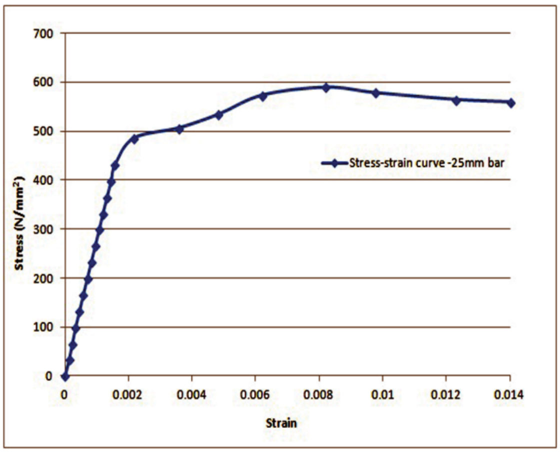

Fig. 5 Stress-strain curve for Fe-415 bar

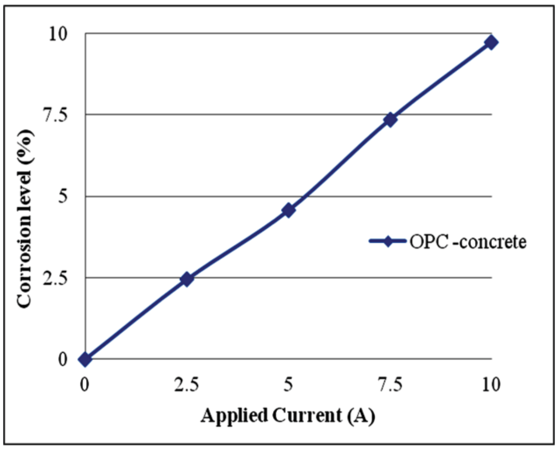

Fig.6 Variation of applied current with corrosion level

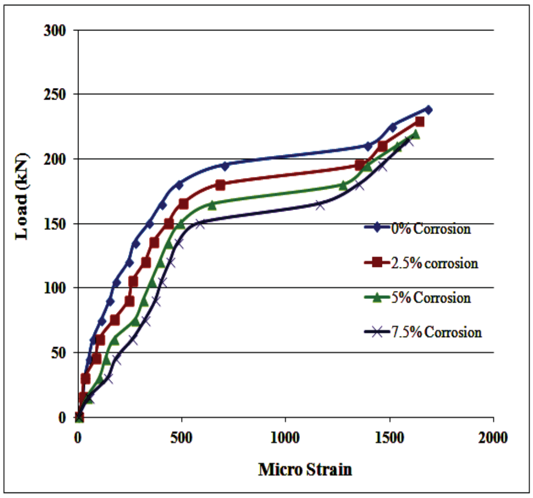

Fig. 7 Effect of corrosion on load strain behavior

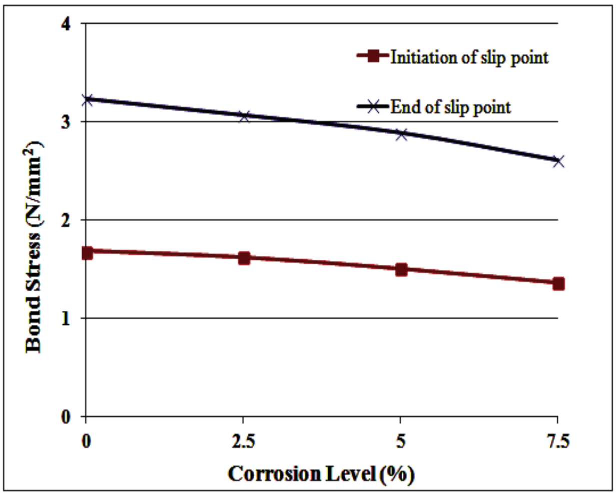

Fig. 8 Effect of corrosion on bond strength

IV. CONCLUSIONS

1. Reinforcement corrosion causes degradation of the bond behavior. The strain value becomes large due to corrosion and the larger the corrosion lesser the bond stress value.
2. Percentage reduction in bond stress for different levels of corrosion i.e. 2.5%, 5%, and 7.5% with respect to control beam specimen are 4.32%, 10.65%, and 18.93% respectively.
3. Bond stress drops for about 2 % (at initiation of slip) and 2.1% (at end of slip point) respectively for every percentage increase in corrosion level.
4. Proposed regression equation is very much useful for quick assessment to predict the bond strength values for different corrosion levels in structure within the range of experimental data**.**

ACKNOWLEDGEMENT

The Partial financial support from Board of Reserch in Nuclear Sciences (BRNS), Govt. of India is gratefully acknowledged.

REFERENCES

[1] S. Bhaskar, B. H. Bharatkumar, G. Ravindra, and M. Neelamegam, “Effect of corrosion on the bond behavior of OPC and PPC concrete,” *Journal of Structural Engineering,* vol. 37, pp. 37-42, Dec. 2010.

[2] *Recommended guidelines for concrete mix design,* Bureau of Indian Standards, New Delhi. IS: 10262, 2009.

[3] S. Ahamad, “Techniques for inducing accelerated corrosion of steel in concrete,” *The Arabian Journal of science and Engineering*, vol. 34, pp. 95-104, Oct. 2009.

[4] M. G. Fontana, *Corrosion Engineering*, Tata McGraw-Hill Education, 2005.

[5] Shetty Akshatha, Katta Venkataramana and Babu Narayan K. S., Flexural bond strength behaviour in OPC concrete of NBS beam for various corrosion levels,” *Structural Engineering and Mechanics, an International Journal*, vol. 49, pp.81-93, Jan. 2014.

A Review: On EDM based Energy Aware Routing Protocol for WSN

Veena Bhat#1, Sharada U Shenoy#2

#Department of Computer Science & Engineering, NMAM Institute of Technolgy , Nitte-574110, Karnataka, India
1veenabhat69@gmail.com
2sharudivardhan@gmail.com

Abstract- **Wireless sensor network are rapidly emerging field in communication with vast arena of applications. Many researches has been carried out in the various sensor network constraints such as routing, power management and data distribution etc., which mainly focus on energy awareness as an essential issue. In this paper we present a review on energy based routing protocols and manifest on a new scheme which portrays on enhancing the efficient utilization of energy and increase network lifetime.**

Keywords- **Wireless sensor network, Energy Efficiency, Power management, Lifetime, Latency, Data accuracy.**

I. INTRODUCTION

A wireless sensor network consists of spatially distributed autonomous sensors to monitor physical or environmental conditions, such as temperature, sound, pressure, etc., to cooperatively pass their data through the network to a main location. The popular network considered in this is to communicate in a multihop manner to control and coordinate network constraints.

The development of wireless sensor networks was motivated by military applications such as battlefield surveillance. A lot of applications of mobile wireless sensor network can be found in different field such as habitat monitoring, wild life tracing, healthcare monitoring, and search and rescue call for mobile sensor networks. Presently these types of networks are foreseen as a horde of applications [1-3].

A Networks main operation is data transfer, so to facilitate communication between the network nodes, a proper establishment of path between source and destination nodes is necessary. This is achieved by the help of routing protocol. Routing in wireless sensor networks is very challenging task due to their distinct characteristics, dynamic in nature, architecture and design issues and resource constraints. A routing protocol is responsible to efficiently perform data transfer function, it mainly concentrated on finding the shortest path between a source and destination node. Figure 1.1 describes the wireless sensor network and its applications.

A. CHARACTERISTICS OF WSN

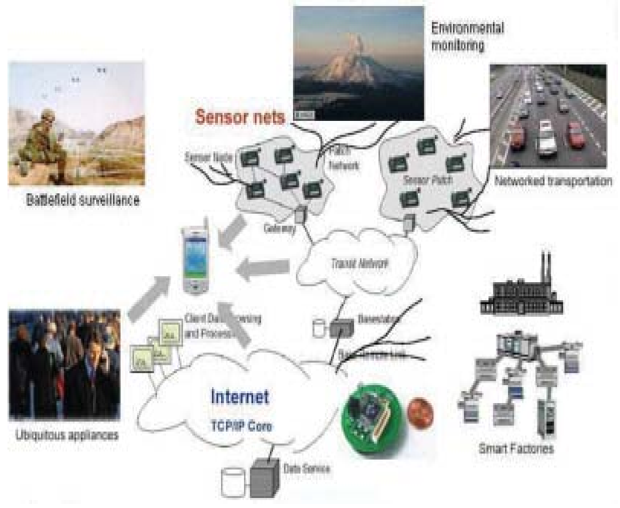

Fig 1.1 Wireless Senor Networks and its applications.

The Main characteristics of Wireless Sensor Networks are listed below.

- *Power consumption constrains for nodes using batteries or energy harvesting*: Sensor nodes are battery operated they consume power, based on the amount of data transfer being done with the routing distance & security applications.
- *Ability to cope with node failures*: Sensor Networks are highly Robust in Nature. Since the nodes are deployed in the real world environment there are possibilities of node failure and destructed due to the environmental changes and effects.
- *Mobility of nodes*: The presence of Nodes in the actual environment provides an easy pathway for its mobility (E.g.; underwater sensors nodes are mobile due to the effect of water currents).
- *Dynamic network topology*: Sensor Nodes deploy themselves in random topology based on the group of nearby nodes & the distance from the Base station.
- *Scalability to large scale of deployment*: The Sensor nodes are characterized efficiently scalable to be deployed in the large scale in the real world environment, in order to support the relevant applications.

- *Ability to withstand harsh environmental conditions*: Sensor Nodes with its characteristic feature of Random deployment and Self-Organizing nature they can tolerate the highly fluctuating environmental conditions on the demand of applications.
- *Ease of use*: This type of Network provides an ease to use and portability and compatibility to any adverse environmental effects.
- *Unattended operation*: These types of Networks are self-monitored hence these nodes can be left unattended by the network manger.

B. *CONSTRAINTS IN WSN*

Individual sensor nodes in a WSN are inherently resource constrained. They have limited processing capability, storage capacity, and communication bandwidth. Each of these limitations is due in part to the two greatest constraints — limited energy and physical size.

• *Energy*: energy consumption in sensor nodes can be categorized into three parts:
–Energy for the sensor transducer
–Energy for communication among sensor nodes
–Energy for microprocessor computation

The study found that each bit transmitted in WSNs consumes about as much power as executing 800–1000 instructions. Thus, communication is more costly than computation in WSNs. Any message expansion caused by security mechanisms comes at a significant cost. Further, higher security levels in WSNs usually require to more energy consumption for cryptographic functions.

• *Computation*: the embedded processors in sensor nodes are generally not as powerful as those in nodes of a wired or ad hoc network.

• *Memory*: memory in a sensor node usually includes flash memory and RAM. Flash memory is used for storing downloaded application code and RAM is used for storing application programs, sensor data, and intermediate computations. There is usually not enough space to run complicated algorithms after loading OS and application code.

• *Transmission range*: the communication range of sensor nodes is limited both technically and by the need to conserve energy. The actual range achieved from a given transmission signal strength is dependent on various environmental factors such as weather and terrain.

C. *ROUTING IN WSN*

In general, routing in WSNs can be classified into flat based, hierarchical-based and location-based routing depending on the network structure. In flat-based routing, all nodes are typically assigned equal roles or functionality. In hierarchical-based routing, nodes will play different roles in the network. In location-based routing, sensor nodes position is exploited to route data in the network. A routing protocol is considered adaptive if certain system parameters can be controlled in order to adapt to the current network conditions and available energy levels. Routing protocols can also be classified into multipath-based, query-based, negotiation-based, QoS-based, or coherent-based routing techniques depending on the protocol operation.

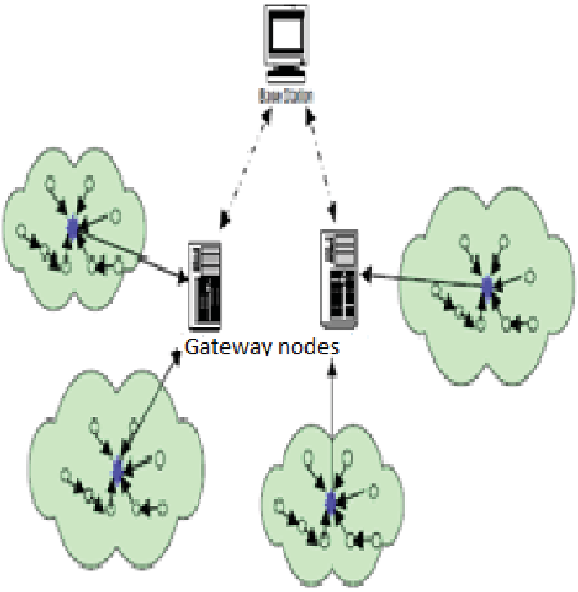

Fig 1.2 Sensor Network Routing Mechanism.

Routing protocols for any wireless networks are broadly classified into three categories, proactive, reactive, and hybrid protocols depending on how the source finds a route to the destination. In proactive protocols, all routes are computed before the actual network communication takes place. In case of reactive protocols, routes are computed on demand. Hybrid protocols use a combination of these two ideas. If sensor nodes are static, then it is preferable to have proactive routing protocols rather than using reactive protocols. A significant amount of energy is used in route discovery and setting up of network. Another class of routing protocols is called the cooperative routing protocols in which nodes send data to a central node where data can be aggregated and may be subject to further processing, hence reducing route cost in terms of energy use. Very few routing protocols rely on timing and position information. Figure 1.2 describes the general routing mechanism prevailing in Wireless sensor networks.

II. RELATED WORKS

Routing in wireless sensor networks is a very challenging errand due to their distinct characteristics, dynamic nature, architecture & design problem and resource constraints. Many researches has been carried out in efficient design of routing protocols, but for Wireless Sensor network design of routing protocol is a major challenge, as it should satisfy many obdurate network constraints.

A routing protocol generally requires updates from path search processes and stores information in the routing table. So, the routing algorithms can affect the processing, memory and energy consumption. Due to limited energy supply, less processing power and memory, the routing algorithms should avoid overheads of storing routing table, re establishment of path search processes during link failure to reduce energy usage.

A cluster-based routing protocol can avoid intensive message exchanges of path search, update processes and overhead of storing routing table or other information that could be expensive. To update typical clustering algorithms, divide WSN nodes into two types: member nodes and cluster heads. The member nodes send data to their cluster-head, then a cluster-head aggregates the data and relays to the base station. Several clustering algorithms have been proposed in this section.

There are various routing protocols proposed and they are summarized in [4, 5]. LEACH [6, 7, and 8] is one of the most popular and promising cluster based protocol and has been widely proposed in WSNs. In [9], a basis to select the optimal probability with which a node should become a cluster head in order to minimize network energy consumption is proposed. They also proposed a sleep-wake up based MAC protocol instead of TDMA for LEACH architecture.

L. Ying et al [10] proposed an energy adaptive cluster head selection algorithm based on node residual energy and energy required for transmission. In [11], energy efficient cluster ID based routing scheme is proposed, and uneven load in network is minimized by cluster size adaptation. The current Cluster head keeps the information of node with maximum remaining energy in its cluster. It ensures the location of Cluster head approximately at center of cluster. In case of uneven deployment it is not necessary that most of the nodes are in center of cluster. So the distance between Cluster head and sensor nodes will be increased. Another protocol presented in [12], consider distance and remaining energy of a node. Base station determines and select appropriate cluster head based on above two parameters. Y. Yin et al [13] proposed a centralized CH selection mechanism based on energy, mobility and distance to cluster centroid and the assumption made is sensor nodes are location perceptive and there is a single-hop communication in a cluster.

The majority of the protocols proposed so far, only consider residual energy for cluster head selection but there are other metrics like distance to aggregation point, node reliability, mobility [20] etc that are also very important in order to maximize network life time. Suitable energy balancing protocols are required to increase scalability, reduce energy consumption and increase the lifetime of the network.

Jia et al., 2007 proposed Hole Avoiding In advance Routing protocol (HAIR). In this approach the hurdles are identified and informed to neighbor nodes before the transaction by a node. In this they can select the path which doesn't have neighbor problems, however to find out the problems and sharing this information among the neighbors needs some energy. More over this method is not suitable for the dynamic environment which consists of mobile nodes.

Hu et al., 2007 proposed to avoid selecting the forwarding node with lower residual battery power than the threshold value. This method could equally balance the total energy consumption between all nodes in the network, but it fails to impart solution where all the nodes receiving the energy less than threshold, makes individual nodes and entire network losses the threshold value in its total running time.

Wang et al., 2007 presented a Local Update-based Routing Protocol (LURP) that allows the sink node to move and update its location information. Since the sensor nodes close to the sink deplete their energy quickly by forwarding messages originating from many other nodes, the nodes which are placed very long to sink node have to communicate with sink through the nodes which are placed near to sink node only. If sensor nodes near to sink node loose its energy quickly it means other nodes are not able to communicate with sink. It results in packet drop and reduces the lifetime of network.

Qiu et al., 2009 presented a tree routing to avoid flooding network with path search and update message in order to conserve energy by using only link information between cluster head and members for packet forwarding. In this technique, only link statuses are verified to avoid the complexity of the message. But this technique does not give the idea about the efficient head selection and load balancing mechanism

Gong et al. 2008 presented an unequal clustering and multi-hop routing scheme to extend the network lifetime of WSNs. In this cluster head selection is based on a cost function which considers the distance and energy usage. Energy usage is not the same in all ranges of transaction and it is depending on distance. But in a dynamic environment distance between the nodes varies based on the mobility of the nodes. So this approach is not suitable for dynamic environment.

Dali & Chan, 2007 proposed a technique to balance and reduce the energy consumption of clustered sensor networks. As the energy consumption of sensor nodes depend on transmission range, the cluster-heads are normally at the center of the cluster. In each cluster, with the highest residual battery level and the node located in the center area is selected as the cluster-head. In real time the possibility of high energy in center node is very less. In case of dynamic environment any node can be placed at any location. But in this method also there is no possibility for center node in all clusters. So this technique proves to be unsuitable for dynamic environment.

Every methods mentioned above are delt in consideration with static network nodes. Do-Seong Kim and Yeong-Jee Chung propose LEACH-Mobile mechanism. The key idea in LEACH-Mobile is to confirm whether a mobile sensor node is able to communicate with a specific cluster head. In this algorithm the protocol transmits a message which requests for data transmission from cluster head and back to mobile sensor node within a time slot allocated in TDMA schedule of a sensor cluster. If the mobile sensor node does not receive the data transmission from cluster head within an allocated time slot according to TDMA schedule, it sends a join-request message at next TDMA time slot allocated for it. Then on reception of join-ack decides the cluster to which it will belong for this moment by receiving cluster join-ack messages back from specific cluster heads.

LEACH-Mobile is focused to confirm the inclusion of sensor nodes in a specific cluster at the steady-state phase as the cluster head and non-cluster head node receives particular message at a given time slot according to TDMA time schedule that each sensor cluster has, and then to reorganize the cluster with minimum energy consumption. LEACH-MOBILE is only focused on cluster formation. It means majority of the work in LEACH-MOBILE is aimed to place the nodes in any one of the cluster.

III. PROPOSED WORK

In this section we provide a brief overview of EDM based cluster head selection, intra and inter cluster communication. Here we provide mobility characteristics to all the participating nodes, except sink node and gateway node. We enable communication among network nodes by a setup phase and steady state phase. Setup phase is responsible for cluster formation and head selection. Steady state phase is responsible for data transaction and routing. NS2 simulator is being used to for simulating the network operations.

Methodology of Proposed work

Our strategy is defined by the following steps.

1. At the initial stage Base station decides the number of network clusters and randomly selects cluster head for all clusters. As all nodes are assumed to have same energy level.
2. Base station broadcasts the request message to get the information of all nodes.
3. Every participating node on reception of request message sends the current details such as node id, residual energy, distance and density to base station.
4. With the received details base station selects an efficient node which has high amount of energy as cluster head. After the selection of head nodes TDMA schedule are created and transmitted to the nodes in the cluster by head node.
5. All the nodes participate in data gathering process.
6. When a sensor node finished data gathering it will send the sensed data to head node of its own cluster.
7. After collecting the data from all sensor nodes head node performing the aggregation process.
8. At the end of aggregation head node transmits the aggregated data to base station through the gate way and other cluster head nodes.
9. At each stage of communication, energy level of nodes will be updated in its memory. Based on this energy and density value efficient cluster head node is selected.

IV. COMPARISION OF EXISTING AND PROPOSED

Head node selection is the main part of increasing the life time of the network. Which means sharing the head role with different nodes and the work load between number of nodes. Energy of all the nodes will deplete in an equal manner, So it will avoid earlier death of individual nodes.

Existing system LEACH-MOBILE is only focused on cluster formation. It means majority of the work in LEACH-MOBILE is aimed to place the nodes in any one of the cluster. It doesn't speak about selection of cluster head.

In our proposed system we mainly focus on efficient head selection. The head node will be selected based on higher residual energy and density. Hence, the higher energy constraint, work load of the node which has the minimum energy will be reduced. And because of the density constraint head node will become easily reachable to all other nodes in cluster. Hence data loss will be minimized. Finally performance of the entire network will be improved by this mechanism.

V. CONCLUSIONS

In this paper we present an overview of different routing protocols used in Wireless Sensor Networks, and portray most of the protocols proposed so far only considering residual energy for cluster head selection but there are other metrics like distance to aggregation point, node reliability, mobility etc that are also very crucial in order to maximize network life time. Appropriate energy balancing protocols are required to increase scalability, reduce energy consumption and enhance the network lifetime of the network on LEACH-Mobile protocol with a new enhancement on classification of cluster head and focus on energy preserving mechanism and hence achieve energy management. Many of these routing techniques look promising; there are still many challenges that need to be solved in the sensor networks.

REFERENCES

[1] I. F. Akyildiz , W. Su , Y. Sankarasubramaniam , E. Cayirci, “Wireless sensor networks: a survey”, Computer Networks: The International Journal of Computer and Telecommunications Networking, v.38 n.4, p.393 -422, 15 March 2002.

[2] J. Yick, B. Mukherjee, D. Ghosal, “Wireless sensor network survey”, Computer Networks: The International Journal of Computer and Telecommunications Networking, Accepted 7 April 2008.

[3] M. Younis, K. Akkaya, M. Eltoweissy, A. Wadaa, “On Handling QoS Traffic in Wireless Sensor Networks”, Proceedings of the Proceedings of the 37th Annual Hawaii International Conference on System Sciences (HICSS'04) - Track 9, p.90292.1, January 05-08, 2004.

[4] K. Akkaya, M. F. Younis: A survey on routing protocols for wireless sensor networks. Ad Hoc Networks 3(3): 325 -349 (2005)

[5] A. A. Abbasi, M. F. Younis: A survey on clustering algorithms for wireless sensor networks. Computer Communications 30(14-15): 2826-2841 (2007)

[6] W. Heinzelman, A. Chandrakasan and H. Balakrishnan, “Energy-efficient communication on systems Sciences, Hawaii, Jan. 2000.

[7] W. Heinzelman, “Application-Specific Protocol Architectures for Wireless Networks," Ph.D. Dissertation, Massachusetts Institute of Technology, June 2000.

[8] W. R. Heinzelman, A. Chandrakasan, and H. Balakrishnan, "An Application-Specific Protocol Architecture for Wireless Micro sensor Networks", IEEE transactions on wireless communications, vol. 1, no. 4, October 2002.

[9] H. Yang, B. Sikdar, "Optimal Cluster Head Selection in the LEACH Architecture", In the IPCCC2007, April 11 -13, 2007, New Orleans, Louisiana, USA.

[10] L. Ying, Y. Haibin, "Energy Adaptive Cluster -Head Selection for Wireless Sensor Networks", Applications and Technologies (PDCAT'05), pp. 634-- 638, 2005.

[11] I. Ahmed, M. Peng, W. Wang, "A Unified Energy Efficient Cluster ID based Routing Scheme for Wireless Sensor Networks-A more Realistic Analysis", Proc of IEEE Third International conference on Networking and Services (ICNS'07), p-86, 2007.

[12] P. Tillapart, S. Thammarojsakul, T. Thumthawatworn, P. Santiprabhob, "An Approach to Hybrid Clustering and Routing in Wireless Sensor Networks", Proc of IEEE Aerospace Conference, 2005.

[13] Y. Yin, J. Shi, Y. Li, P. Zhang, "Cluster-Head Selection using Analytical Heierarchy Process for Wireless Sensor Networks", The 17th Annual IEEE International Symposium on Personal, Indoor and Mobile Radio Communications (PIMRC'06), China.

[14] H. Hsu, Q. Liang, "An Energy-Efficient Protocol For Wireless Sensor Networks", In proceedings of 62 nd IEEE Vehicular Technology Conference, 2005, vol.4, pp -2321-2325.

[15] A. A. Minhas , "Power Aware Routing Protocols for Wireless ad hoc Sensor Networks" , Ph. D Thesis, Graz University of Technology, Graz, Austria, March, 2007.

[16] L. Hu, D. Evans, Localization for mobile sensor networks, ACM International Conference on Mobile Computing and Networking (MobiCom 2004), 2004.

[17] J. Hightower, G. Borriello, Location systems for ubiquitous computing, IEEE Computer 34 (8) (2001) 57–66..

[18] G. Hoblos, M. Staroswiecki, A. Aitouche, Optimal design of fault tolerant sensor networks, IEEE International Conference on Control Applications, Anchorage, AK, September 2000, pp. 467 –472.

[19] U. B. Desai, B. N. Jain, S. N. Merchant, "Wireless Sensor Networks: Where do We Go?", www.ee.iitb.ac.in/spann.

[20] G. Ahmed, N. M. Khan, R. Ramer, "Cluster Head Selection Using Evolutionary Computing in Wireless Sensor Networks", Progress In Electromagnetics Research Symposium, Hangzhou , China, March 24-28, 2008.

DCT Based Watermarking Method in HSV Color Space

Anupama V [#1], Venugopala P S [#2], Sarojadevi H [#3] and Niranjan N Chiplunkar [#4]

[#] *Department of CSE, NMAM Institute of Technology, Nitte, Udupi,Karnataka, India*
[1]`anupamavbhat@gmail.com`
[2]`venugopalaps@gmail.com`

Abstract - **In this paper a simple watermarking method for color images is proposed. The proposed method is based on watermark embedding in HSV planes using Discrete Cosine Transform (DCT) transformation. First, the Digital Color Image is transformed into HSV from RGB color space and then the DCT middle band of the each (Hue, Saturation and Value) component is used for watermarking processes. Voting is used to extract the best candidate pixel value. The results demonstrate the robustness of the technique against various types of attacks.**

Keywords- **Digital Watermarking, DCT, RGB Color Space, HSV Color Space**

I. INTRODUCTION

The rapid expansion of networked multimedia systems has added on the need for image copyright protection. Digital watermarking is a potential method to address problem of copyright protection, content usage and illegal replication.
Digital Watermarking can be defined as a technology of embedding data called a watermark or digital signature or tag or label into a multimedia object such that watermark can be detected or extracted later to make an assertion about the object[1-6].

Digital watermarking can be categorized into different types based on different basis [1]. Watermarking techniques can be divided into image, audio, text, video according to the type of document to be watermarked. According to the human perception, the digital watermarks can be divided into visible, invisible and dual watermark. The watermark appears visible to a viewer on inspection where has invisible watermark is not visible to the viewer. Dual watermark is the combination of visible and invisible. According to working domain watermarks can be applied in spatial domain and frequency domain. In spatial domain watermarking is applied directly by altering the pixel values. In frequency domain transformation like DCT, FFT, DWT are applied to image and values of selected frequencies are altered.

Watermarking system consists of three parts: watermark, encoder (insertion algorithm) and decoder (verification or extraction or detection algorithm). . Watermark may be text, logo, image or binary digits.

A. Overview of DCT

The DCT allows an image to be broken up into different frequency bands, making it much easier to embed watermarking information into the selected frequency bands of an image. The middle frequency bands are chosen such that they avoid the most visual important parts of the image (low frequencies) without over-exposing themselves to removal through compression and noise attacks (high frequencies) [2].
Two dimensional discrete cosine transform (2D-DCT) is defined as [3]

$$F(u,v) = \alpha(u,v) \sum_{x=0}^{N-1} \sum_{y=0}^{N-1} f(x,y) cos\left[\frac{(2x+1)u\pi}{2N}\right] cos\left[\frac{(2y+1)v\pi}{2N}\right]$$

Where F (*u*, *v*) is the resulting DCT coefficient at the coordinates (*u*, *v*), *f* is the two dimensional square array of size *N* × *N and* $\alpha(u, v)$ is defined by

$$\alpha(u,v) = \begin{matrix} 1/N & for\ u = 0\ and\ v = 0 \\ 2/N & otherwise \end{matrix}$$

The corresponding inverse transformation (2D- IDCT) is defined as

$$f(x,y) = \sum_{x=0}^{N-1} \sum_{y=0}^{N-1} \alpha(u,v) F(u,v) cos\left[\frac{(2x+1)u\pi}{2N}\right] cos\left[\frac{(2y+1)v\pi}{2N}\right]$$

B. HSV Color Space

HSV is the most common cylindrical-coordinate representations of points in an RGB color model. HSV stands for hue, saturation, and value. While working on coloured images when using the mathematical and biological models of Human Visual System, the preferred colour model must be HSV color model rather than RGB color model because it most closely defines how the image is interpreted by Human Visual System [4].

II. PROPOSED METHOD

The Digital Color Image is transformed into HSV from RGB color space and then the DCT middle band of the each (Hue, Saturation and Value) component was used for watermarking processes.

A. Embedding Process

In the proposed method first image is transformed from RGB color space to HSV color space. Then each component is divided into 8x8 DCT blocks located at different positions. For example if we start with the top left corner block in the Hue component, we will use the bottom right corner block in the Saturation component and other different location for the Value component. The next step is to perform the DCT on each three corresponding blocks.

Two locations $B_i (u_1, v_1)$ and $B_i (u_2, v_2)$ are chosen from the middle frequency region for comparison. The DCT block will encode a “1” if B_i (u1, v1) > B_i (u2, v2); otherwise it will encode a “0”. The coefficients are then swapped if the relative size of each coefficient does not agree with the bit that is to be encoded [2].

For example let the two location chosen be (5, 2) and (4, 3) then if the watermark bit equals to 1 then the DCT coefficient location for (5, 2) is expected larger than the DCT coefficient for (4, 3). If the bit is 0 then the DCT coefficient for (4, 3) is expected larger than the DCT coefficient for (5, 2).

Finally IDCT is applied and image is reformed. Figure 1 shows the outline of the embedding algorithm.

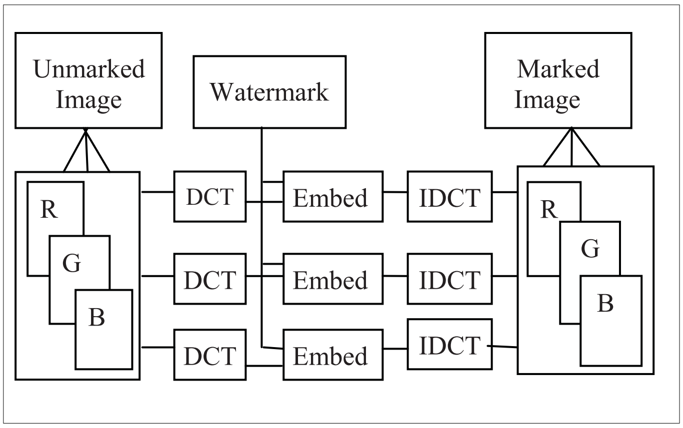

Fig. 1 Embedding flow Chart

B. Extraction Process

First image is transformed from RGB color space to HSV color space. Then HSV color components are separated. Then each component is divided into 8x8 DCT blocks located at different positions. Then watermark bits are extracted by applying DCT on each three corresponding blocks and comparing two selected location coefficients (same like embedding process). Extracted bits of each component (Hue, Saturation and Value) are passed through the voter get final bit. Voter is designed such that it outputs one if there is two or more ones and outputs zero if there is two or more zeroes. Figure 2 shows the outline of the extracting algorithm.

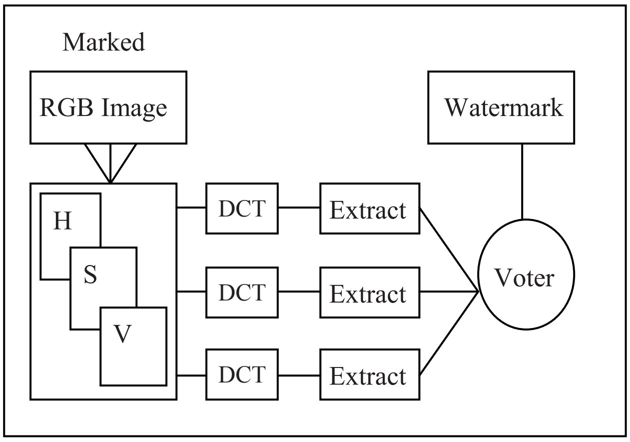

Fig. 2 Extracting flow Chart

III. EXPERIMENTAL RESULTS

In the experiments, standard “Lena” color image [7] with the size of 512×512 pixels were used as the original image. The binary image of size 16x256 is used as watermark. In all experiments, The quality of watermarked image by measuring its *PSNR* (Peak Signal-to- Noise Ratio) and the quality of extracted watermark was evaluated by measuring its *NCC* (Normalized Cross-Correlation). For both measuring methods, the higher value indicates a better quality of the results obtained.

In this experiment, the performance of proposed method has been evaluated for being compared with the previous method in [2]. The experimental results in Table 1 show that the proposed scheme has higher robustness, especially for against noise and higher ratios of JPEG compression.

TABLE I
RESULTING PSNR AND NCC VALUES FOR VARIOUS ATTACKS

Attack	**Proposed Method**		**Previous Method**	
	PSNR	**NCC**	**PSNR**	**NCC**
Without any Attack	42.88	1	41.22	1
Cropping borders of size 20 pixels	31.56	0.9267	31.23	0.9098
Normal distributed noise (0-10)	30.14	0.8654	30.17	0.8583
JPEG compress with quality 50	28.97	0.8796	28.74	0.8770
JPEG compress with quality 75	30.01	0.8858	29.59	0.8830

IV. CONCLUSIONS

An image watermarking algorithm for copyright protection based on the discrete cosine transform in HSV color space is presented in this paper. The process of the proposed algorithm, including watermark embedding, and watermark detection, is described in detail. We summarize the features of the proposed method as follows:

- Watermark is embedded in HSV color space.
- During extraction voter is used to get accurate watermark.
- The method has been proved to be robust against, cropping, noise addition and jpeg compression with good NCC values.

REFERENCES

[1] Saraju P. Mohanty, "Digital Watermarking: A Tutorial Review".

[2] El-Fegh, D. Mustafa, Zakaria Suliman Zubi, Faraj A. El-Mouadib "Color Image Watermarking based on the DCT-Domain of Three RGB Color Channels", roceedings of the 10th WSEAS International Conference on Evolutionary Computing.

[3] Mona M. El-Ghoneimy, "Comparison Between Two Watermarking Algorithms Using DCT Coefficient, and LSB Replacement", Journal of Theoretical and Applied Information Technology.

[4] Piyush Kapoor, Krishna Kumar Sharma, S.S. Bedi, shwani Kumar, "Colored Image Watermarking Technique Based on HVS using HSV Color Model", ACEEE Int. J. on Network Security , Vol. 02, No. 03, July 2011

[5] Komwit Surachat, "Digital Watermarking using a Multiple Signals Embedding Technique and Cropping Detection Algorithm in HSV and YIQ Color Spaces", ICEEI 2012.

[6] Rawan I. Zaghloul, Enas F. Al-Rawashdeh, "HSV Image Watermarking Scheme Based on Visual Cryptography", World Academy of Science, Engineering and Technology 44 2008.

[7] "Set of Classical Test Images" [Online].Available: http://www.hlevkin.com/TestImages/classic.htm.

Design and Development of an Anthropomorphic Foot for Humanoid Robot

B. Karthikeya Kamath[#1], Sang-ho hyon*[2] and Muralidhara[#3]

[#]Department of Mechanical Engineering,NMAM Institute of Technology, Karkala, Karnataka, India
*Graduate School of Science and Engineering, BKC, Ritsumeikan University,
[1]karthikeya.kamath7@gmail.com
[2]gen@fc.ritsumei.ac.jp
[3]mr_kallya@yahoo.com

Abstract— **About half of the Earth's landmass is currently inaccessible by wheeled or tracked vehicles, whereas legged animals can move easily. To achieve the stable biped walking through steady interaction with any rough terrain, robot's foot should have the structural flexibility that mimic's the human's foot. The paper presents mechanical design of a new biped foot system integrated with a ground contact sensor to overcome the issues of biped walking on rough terrain. The ground contact sensor and its working is explained briefly, while the foot mechanism design which complements the sensor is presented with full details. The design limitations and specifications are reported and the design criteria cum selection of mechanical components are closely examined. Important functions like shock absorption are included in the design with low cost approach. The 3D drawing of final assembly and simulation results are incorporated.**

Keywords— **Humanoid robot, Anthropomorphic foot design, Ground contact detection, Impact absorption.**

I. INTRODUCTION

Humanoid robots nowadays are capable of performing various human like movements such as walking, running, turning and stairs climbing. However, most of the movements are achieved in laboratory environment, with flat and smooth floor. In order to utilize humanoid robots in assisting our daily jobs, they must be able to move smoothly in human's living environment, which include inclined slope and rough terrain like tarred road. Human foot has a great ability of adapting to the contours on the ground [1] absorbing shock and impact force [1] and storing and releasing energy to increase locomotion efficiency [2]. With an anthropomorphic approach of mimicking the design of human foot, this ability can be impregnated in to biped foot.

There are fewdesign approaches on anthropomorphic humanoid robotic feet for greater efficiency and encountering uneven surface. Basically, they can be divided into four categories: Tactile sensing [3], multi degree of freedom [4, 5] and multi-sensory feedback and shock absorbing [7].

The tactile sensing method is useful in collecting the ground information, for example slope and irregularity by using a few pressure sensors [3] or constant scanning of a pressure sensor grid. The peak pressure values obtained from the readings indicate the contact point of foot with ground which can be used in the gait control.

For foot design with multi degree of freedom, it aims to provide to provide better grip and stability for the robot on the irregular shape of uneven terrain. Design from Yang utilized flexible cable to change the shape of the foot by manipulating the orientation of four metal plates that formed the foot of robot [4].While Hashimoto designed an interesting robotic feet that have cam-type locking mechanism which guarantees the robot to maintain four-point contact on the ground while walking [5]. Besides that, an arc-shape foot is a relatively simpler mechanism from Minakata to give compliance to the shape of uneven terrain [6].

In order to achieve more accuracy in decision making for uneven terrain walking, multiple sensors like MEMS accelerometer and angular rate gyroscopes can be installed to foot of biped robot. Other than that, multiple layers of shock absorbing rubber pads are sandwiched between top and bottom plates of WAF-2 to permit a small angle of inclination between the foot structures itself [7]. Besides that, another approach to uneven ground walking is by using tools. HOAP-3 from Tokyo Denki University was demonstrated to walk across uneven terrain with the help of a stick [8].

This paper presents a new foot system for biped walking on rough terrain and its design flow. To achieve the stable biped walking on rough terrain, the foot is integrated with differential air pressure sensors to detect ground contact, which is crucial to initiate an appropriate response. Our aim was to design a robot foot with an anthropomorphic approach and integrate it with a ground contact sensor that is very sensitive and tough so that it can sustain uneven terrain easily. The proposed foot is able to not only adapt to rough terrain but also absorb the impact force and the influence of disturbance. The performance of the foot and sensor will be tested on H1 humanoid robot shown in Fig 1, which has fourteen DOF (Degrees Of Freedom) in total, 2 DOF in trunk portion and each leg has 6 actuated (DOF). It is about 140 cm tall and weighs less than 65 kg. Joint torque at each joint is provided by single ended hydraulic cylinder and to reduce total weight, the links between the joints are entirely made by carbon fibre reinforced polymer tubes. Potentiometers are attached at the active joints to determine the joint position and force sensors are mounted on each actuator to determine the force and torque value. A gyro sensor used to for maintaining the balance of the robot. The range of motion of each joint is similar to that of humans and is specified in Table 1.

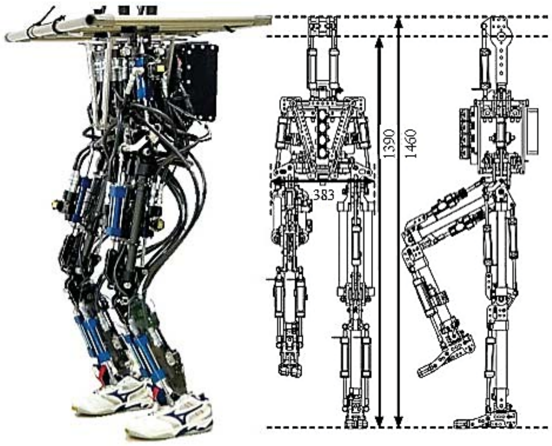

(a) (b)

Fig.1 (a) Humanoid robot H1 (b) CAD model [9]

TABLE I

LIST OF JOINTS AND THEIR SPECIFICATION

	Joint	ROM (deg)	Max Torque (Nm)	Max Velocity (deg/s)
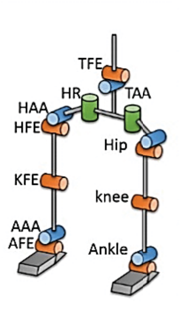	TFE	-50/50	-	
	HFE	-100/30	360	-
	KFE	0/130	345	1370
	AFE	-50/50	734	1300
	TAA	-15/15	-	-
	HAA	-25/80	405	820
	AAA	-15/15	830	830
	HR	-20/20	440	820

The paper is organized as follows. Development of Foot Mechanismis introduced in Section II. Here we formulate a method for ground contact detection and absorption of landing impact. In Section III actual design and analysis is discussed before fabricating the modelIn Section IV results from the various analysis and 3D foot model are incorporated .In Section V Finally paper ends with conclusion and few words on future works.

II. DEVELOPMENT OF FOOT MECHANISM

In this section we discuss upon anthropomorphic approach in developing foot mechanism that not only provide a mechanically stable configuration under uneven terrain condition, but also reduce impact. By studying at human feet and walking biomechanics, features for stable walking are extracted to be applied on this foot mechanism.

Before starting on the detailed designs of the foot mechanism, the basic dimension was first determined to serve as a reference and starting point of the design. In order to create a biped robot foot that is human-like, anthropometric data was referred and used in the design [10]. Taking the anthropometric data of Asian, Japanese men to be specific, the mean body height is 1688mm while foot length and breadth are 251mm and 104mm respectively. Since the height of H1 robot is 1450mm, taking the foot size proportionately, the dimension of H1 foot should be 215mm x 117mm. Conceptual design for the foot was started from this dimension, however, due to installation of mechanical components and safety consideration, the final dimension of foot developed is 290mm x 117mm which is as shown in the Fig 2.

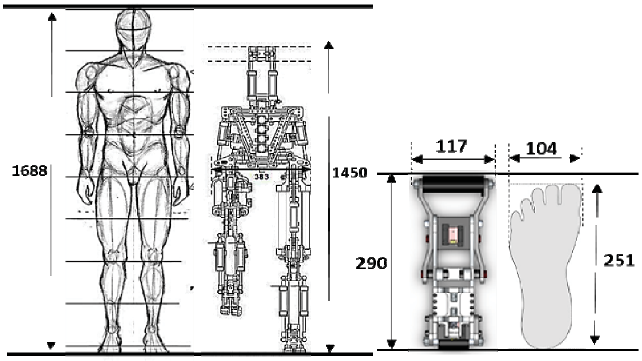

Fig.2 Comparison of human anthropometric data with H1 robot size

2.1 Design specification

Human rely on sensory systems like vestibular organs, proprioceptive receptors, exteroceptive tactile sensor (pressure) and vision, to maintain dynamic balance during locomotion. These sensory feedbacks are rapidly processed by the central nervous system with high accuracy [11]. The mapping of above human sensory organs to mechatronics hardware is as below: Vestibular organs balance human posture, it can be represented by gyroscope. Proprioceptive receptors provide sense of the relative position of neighbouring parts of body. It can be represented by strain gauge and exteroceptive tactile cues provide sense of touch/pressure which can be represented by the same, while vision system can be represented by camera.

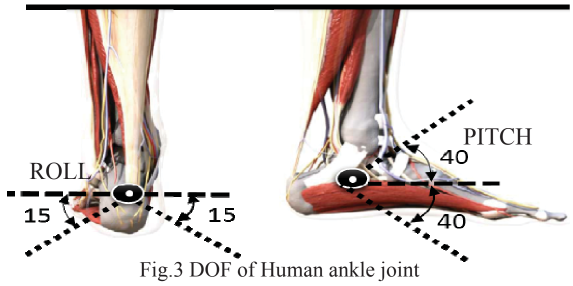

Fig.3 DOF of Human ankle joint

Taking away vision system and vestibular organs which are not available on foot, we can conclude specifications as,

(I) Exteroceptive to detect foot landing and obstacles.
(II) Proprioceptive to sense torques acting on the foot.
(III) The most important part in the foot is the ankle joint which has 2DOF, pitch and roll as shown in Fig 3.
(IV) Besides that, the structure of human foot contributes to safe and comfortable locomotion, where arches of foot support the body weight and absorb Impact, thus a shock absorption mechanism is required.
(V) Maximum heel-contact and toe-off motion of 30°.
(VI) Maximum walking speed of 3ms^{-1}.
(VII) Average man's foot (size 9.5) weighs approximately 1.04 kg (2.3lbs) [12]. Weight of foot should not be too heavy, heavy foot will increase the impact and delays the reflex time. Thus 1kg of maximum permissible foot weight was decided.

2.2 Selection Criteria

1) Criteria for shock absorption:

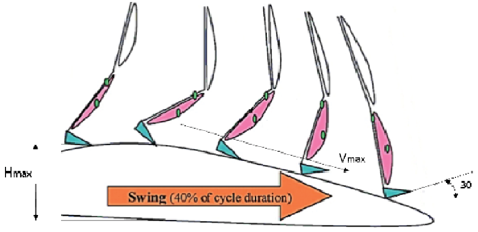

Fig.4 End of swing phase

Considering worst case falling scenario during walking, the required degree of shock absorption can be determined. The worst case scenario happens during single support phase, where the lifting foot reaches highest point and swinging with maximum speed as shown in Fig 3. Hence, the maximum impact energy,

$$E_I = 0.5mV_s^2 + mgh \qquad (1)$$

Leg swinging phase for single support is normally taken to be 40% of the cycle time. Hence, for maximum walking speed, V_{max}, the maximum leg swinging speed,

$$V_s = 0.4V_{max} \qquad (2)$$

Thus, taking maximum value of 9kg for the weight of the foot and leg with 8cm for the step height, the maximum impact energy is 13.54J.In order to prevent damages the shock absorption mechanism on foot must be able to absorb minimum of 13.54J.

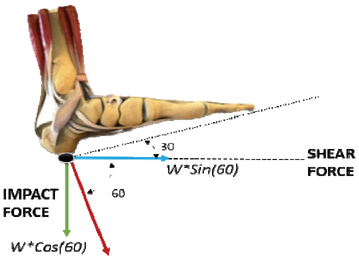

Fig.5 Forces resolved in heel strike

Figure 5 describes the resolved forces during heel strike. With H1's weight of 65kg and maximum angle of inclination 30°, the impact force generated by foot during heel contact is given by ,

$$F_{impact} = WCos60° (3)$$

This Impact force is calculated for normal stance while walking. Force value tend to increase by 3 to 5 time depending on waking or running speed and uneven terrain .Thus considering safety 2250N of impact force was used to calculate the deformation caused by this impact force to make the foot come to rest .a deformation of about 6mm was obtained by using following relation.

$$E_I = F_{impact} * S \qquad (4)$$

2) Criteria for Shear absorption:

During the heel-contact there will also be huge shearing force acting horizontally in the foot structure. With H1's weight of 65kg and maximum angle of inclination 30°, the shearing force, F_{shear} can be determined from geometrical relationship, which has maximum value of 319N.

$$F_{shear} = Wsin30° \qquad (5)$$

III. DESIGN AND ANALYSIS

The design of the H1 feet is divided into three stage. First stage is connected to the bottom part of CFRP tube and hydraulic actuators .The middle Stage is the backbone of the foot which holds vertical plates together while bottom layer consists of 2 separate sensors to detect firm landing of robotic foot which is as shown in Fig 6.

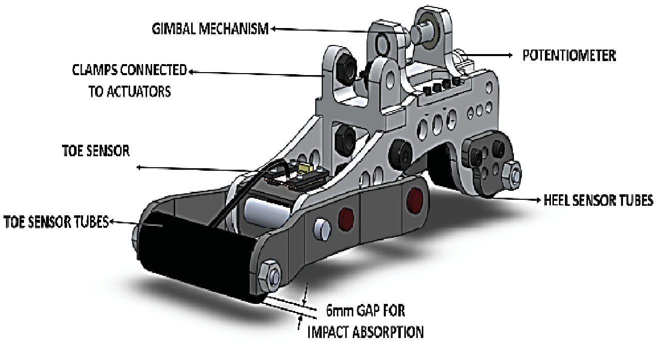

Fig.6 CAD model of H1foot.

3.1 Ankle joint design

The load carrying construction of the ankle joint consists of a gimbal mechanism that helps the ankle to roll and pitch. A set of aluminium cross axles connected to the bracket through the gimbal and a spherical bearing is shown in Fig7 .The ankles comprise of two actuated axes which are secured by clamps.

Aluminium pulleys are mounted at 2 mutually perpendicular ends of the cross axles, which are in turn connected to potentiometer through belt. This plays major role is determining the joint angle variation during control. The right/left ankles are made from identical components, which make them simple and easy enough to manufacture.

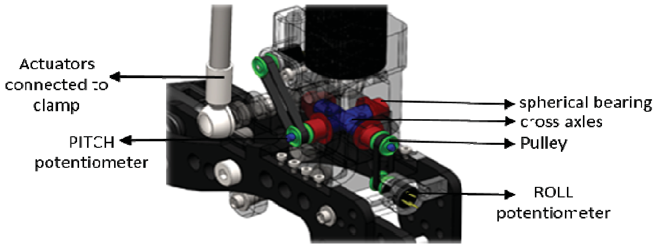

Fig.7 Ankle design.

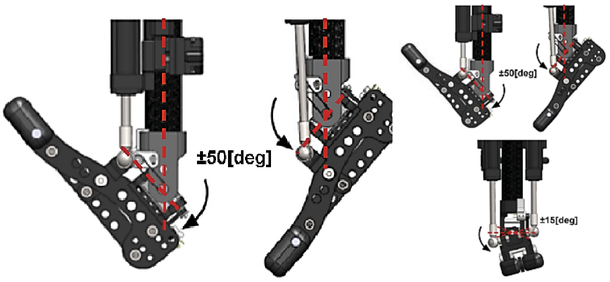

Fig.8 DOF for ankle joint

Ankle joint has 2DOF, with maximum rotation of 50 degree in roll direction and 15 degree in pitch direction as shown in Fig 8. Since parallel hydraulic actuators are attached to the foot with the help of linkball, controlling of these DOF becomes more smooth and convenient.

3.2 Anthropomorphic Feet design

The feet design consists of milled aluminium plates. The overall topology is given by the 2 parallel plates, which is assembled by clamps and two supporting rods as shown in Fig 9. The design of the milled plates have a very close resembles with human skeleton, thus under compressive load it acts as a flexible spring.

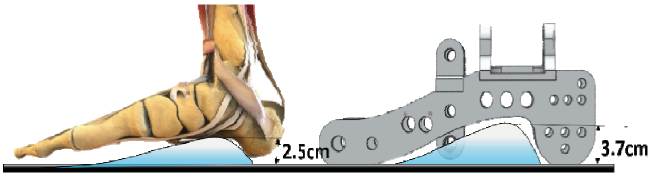

Fig.9 Anthropomorphic Feet design

3.3 Sensor design

To integrate sensor on the robot foot and determine the ground contact we have used a simple concept of Boyle's law which states that – "The absolute pressure exerted by a given mass of an ideal gas is inversely proportional to the volume it occupies if the temperature and amount of gas remain unchanged within a closed system"

Mathematically, Boyle's law can be stated as

$$P \propto 1/V \quad (6)$$

Where P is the pressure of the gas, V is the volume.

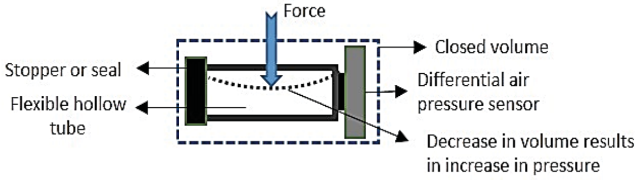

Fig.10 working principle of the Ground contact sensor

Figure 10 describes the working principle of the Ground contact sensor .To detect the contact, a closed volume is created by connecting the sensor to one end of the flexible hollow tube and the other end of tube is sealed. Whenever a force acts on this flexible pipe, it compresses. This in turn increases the pressure inside the tube due to closed volume. The sensor detects this pressure change there by the contact is determined.

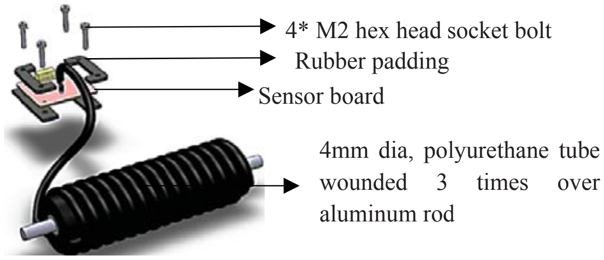

Fig.11 Exploded view of sensor unit with soft tube

The entire gait phase is defined based upon 2 aspects, the heel strike (point of initial contact of the foot on to the ground) and the Toe strike (the point where the foot will go off the ground). Thus heel and toe part of the foot are the ideal position for these sensors to be mounted. And since these tubes are wounded upon a shaft, the contact can be detected not only in vertical direction but any obstacle in fore or rear direction pressing against these tube can be sensed. Thus making these sensors a promising one to be used in uneven terrain.

3.4 Shock Absorption Elements

In this case soft polyurethane tube is used as the flexible hollow tube with 4*2.5 diameters which is shown in Fig10. In order to sustain the robot weight of about 70 kg and to maintain the sensitivity of the sensor, the tubes were wounded 3 times over each other upon 12mm diameter aluminium rod. This damping tube assembly is mounted in such a way that the distance between the outer most diameter tubes and lower portion of the foot is exactly 6mm. During impact this gap enables the tube to absorb all the energy.

3.4 Design Analysis

Each stage of design is analysed through FEM tool and optimised to get best results. In order to determine various stress and strain in the structure, we developed 3 different analysis based on the stance phase of gait cycle. The basic human gait cycle consists of stance phase and the swing phase which is as shown in Fig 12.

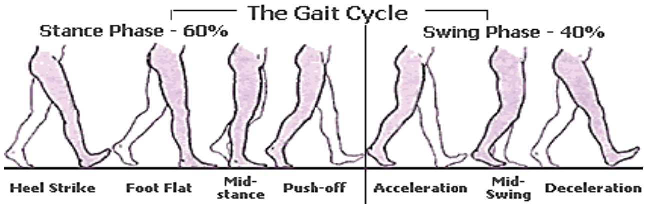

Fig.12 Basic Gait cycle

A. *Impact Analysis*

The initial point of every gait cycle is heel strike. During this, heel comes in contact with ground at certain velocity causing a huge impact. The angle at which the heel strikes the ground depends on the velocity of walking. In an average human foot strikes the ground at about 3m/s while walking [13]. During heel strike the angle between ground and foot is about 30 degrees [13]. These 2 factors are considered as the boundary condition for the impact analysis which is shown in Fig 13.

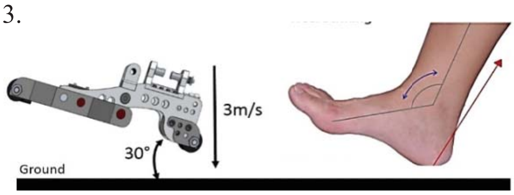

Fig.13 Impact analysis for heel strike

B. *Static Analysis*

During foot flat and mid stance of the gait cycle both heel and the toe will be in contact with ground which is as shown in Fig 14. Entire weight of the body is distributed between heels and toe, thus can be treated as the condition of force acting on a simply supported beam. The robot weighs about 600N and considering safety of the design 2000N force was applied on the brackets of gimbal mechanism.

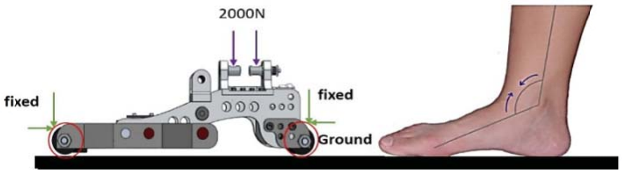

Fig.14 Static analysis for mid stance

C. *Nonlinear Analysis*

Foot off is the final point of the stance phase in gait cycle. During this a large amount of force acts upon the toe just before it leaves the ground which is as shown in Fig 15. Nonlinear analysis will give us an idea how much the tubes of the sensor will deform during the Foot off. Due to the axial symmetry of the sensor the analysis is made simple by creating a 2D model.

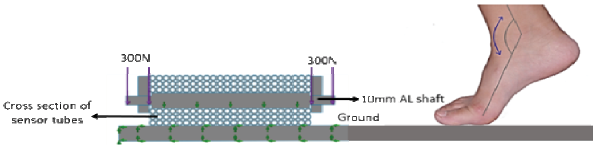

Fig.15 Nonlinear analysis for toe off

IV. RESULTS

A. *Roll and Pitch Analysis*

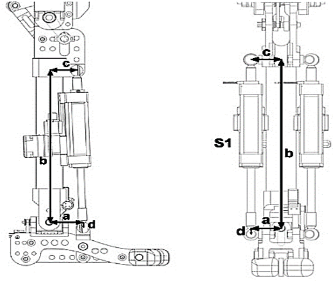

(a) (b)

Fig.16 analysis of (a) pitch (side view)(b) roll (front view)

S1 and S2 are the 2 hydraulic cylinders which control the pitch and roll motion of the foot which is as shown in Fig 16. When both S1 and S2 operates simultaneously the foot will operate in pitch direction and when S1 and S2 independently it operates as the roll. Table 2 gives the specification of the different parameters that is necessary to define the pitch and roll motion. Figure 17 shows the variation of the angle with stroke length during pitch and roll.

TABLE II

PARAMETERS OF ROLL AND PITCH ANALYSIS

Parameter	Length (m)
a	0.05
b	0.282
c	0.04
d	0.01

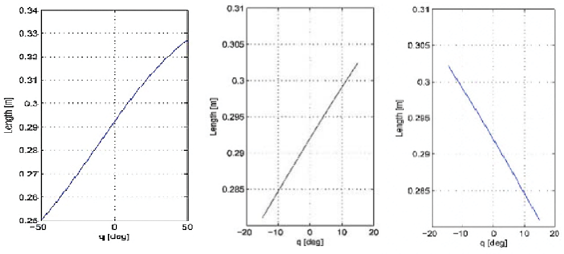

(a) (b) (c)

Fig.17 Parameterb VS Angle for (a)Pitch (b) S1-roll (c) S2-roll

B. *Impact Analysis*

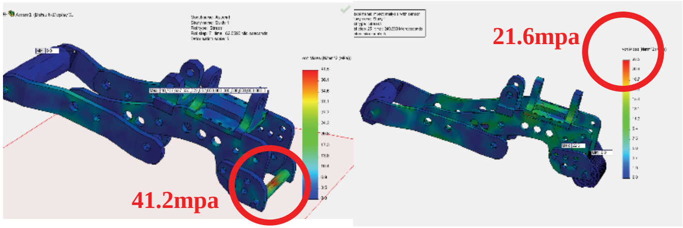

(a) (b)

Fig.18 Impact analysis (a) without sensor tubes (b) with sensor tubes

Figure 18 impact analysis results shows that, by the integration of the sensor tubes upon foot, the large amount of stress (41.2MPa) induced can be reduced up to 50%. These results were obtained exactly after 500milliseconds of impact.

C. *Static Analysis*

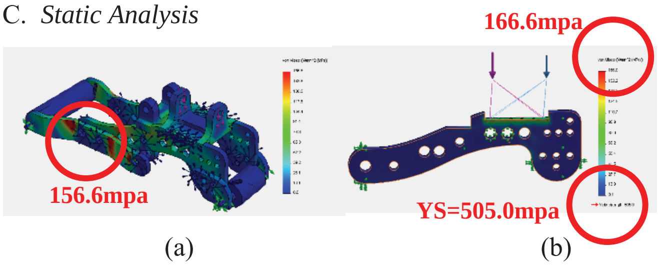

(a) (b)

Fig.19 Static analysis (a) assembly (b) parallel foot plate

Static analysis was performed by applying fixed supports to the toe and heel sensor. This will help us to understand how a force of 2000N will generate stress and deformation in various parts. Figure 19(a) shows that maximum stress of 156.6MPa was generated at toe sensor support. To understand the stress distribution on parallel foot plates a static analysis on single foot plate was carried out with similar boundary condition. The results obtained are as shown in Fig 19(b).Analysing these results we can conclude that the design of foot had a FOS of 3 for a max load of 2000N.

D. *Nonlinear Analysis*

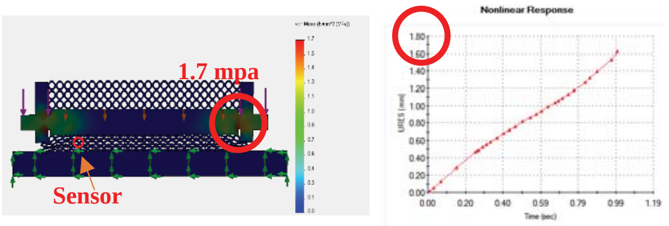

(a) (b)

Fig.20(a) 2D assemblyanalysis (b) Strain VS Time

Nonlinear analysis will helps us understand the deformation of viscoelastic soft polyurethane tubes under constant load condition .The results obtained from this analysis are shown in Fig 20(a). A measurement sensor was defined upon the cross section of tube, which will allow us to get the time response. Figure 20(b) shows that the deformation of tubes is nonlinear and have a max deformation of 1.62mm at the end of one second loading. This deformation is for single turn, but when the number of turns increases the deformation also increases. For 3 turns,5.2mm of total deformation was obtained by the end of this analysis.

V. CONCLUSIONS

To achieve the biped walking on rough terrain, it is necessary to stabilize the contact state between the foot and the ground. However, the contact state changes easily and the foot is separated from the ground in case of the conventional rigid and flat foot. We have presented a new footsystem that has the following advantages: 1) Ground contact detection and 2) Absorption of the landing impact.

The foot was designed with an anthropomorphic approach. The foot has 2DOF (pitch and roll) with potentiometers attached to determine the joint angle movements. The sensor tube deformation results obtained from the theoretical calculation fairly match with the FEM Impact simulation results. Further to optimize the foot design static analysis and dynamic analysis were also carried out.

In the future, the proposed foot will be integrated with an active toe for more stable walking and also the arch will be made from a new mechanism that will enhance the flexibility of foot.

VI. ACKNOWLEDGMENT

Authors of this paper would like to thank Mr.DaisukeSuewaka and Mr. Atsutoshi yagi of Ritsumeikan University, for their help in mechanical design of the foot and circuit design for the sensor.

REFERENCES

[1] L. Klenerman, B.A. Wood, N.L. Griffin. “The Human Foot”. Pub. *Springer*. 2006.

[2] G.M. Humphry. “The Human Foot and Human Hand”. Pub. *Macmillan* and Co. 1861.

[3] Suwanratchatamanee, K., Matsumoto, M., Hashimoto, S.: A Simple Tactile Sensing Foot for Humanoid Robot and Active Ground Slope Recognition. In: *IEEE International Conference on Mechatronics*, April 14-17, pp. 1–6. IEEE Press, New York (2009)

[4] Yang, H., Shuai, M., Qiu, Z., Wei, H., Zheng, Q.: A Novel Design of Flexible Foot System for Humanoid Robot. In: *IEEE Conference on Robotics, Automation and Mechatronics*, pp. 824–828 (2008)

[5] Hashimoto, K., Hosobata, T., Sugahara, Y., Mikuriya, Y., Sunazuka, H., Kawase, M., Lim, H., Takanashi, A.: Development of Foot System of Biped Walking Robot Capable of Maintaining Four-point Contact. In: *IEEE/RSJ International conference on Intelligent Robots and Systems*, pp. 1361–1366 (2005)

[6] Minakata, H.: A Study of Flexible Shoe System for Biped Robot. In: The 8th *IEEE International Workshop on Advanced Motion Control*, pp. 387–392 (2004)

[7] Yamaguchi, J., Takanishi, A., Kato, I.: Development of a Biped Walking Robot Adapting to a Horizontally Uneven Surface. In: Proceedings of the *IEEE/RSJ/GI International Conference on Intelligent Robots and Systems* 1994. Advanced Robotic Systems and the Real World, vol. 2, pp. 1156–1163 (1994)

[8] Shimizu, H., Wakazuki, Y., Pan, Y., Furuta, K.: Biped Walking Robot Using a Stick on Uneven Ground. In: *Annual Conference SICE*, pp. 83–88 (2007)

[9] D.Suewaka, H.Ishida,S.H. Hyon, “Hydraulic Lightweight Biped Robot, Part I:Mechanical design" in proc.2013 *Japan fluid power system society spring conference*, pp 28-30.

[10] Marras, W.S., Karwowski, W.: Fundamentals and Assessment Tools for Occupational Ergonomics. *RC Press*, Boca Raton (2006)

[11] Kumar, S.: *Biomechanics in Ergonomics*. Taylor & Francis, Philadelphia

[12] [online]. Available: http://www .en.wikipedia.org/wiki/Foot

[13] Dario, P.; Laschi, C.; Carrozza, M.C.; Guglielmelli, E.; Teti, G.; Massa, B.; Zecca, M.; Taddeucci, D.; Leoni, F. "An integrated approach for the design and development of a grasping and manipulation system in humanoid robotics", *Intelligent Robots and Systems, 2000. (IROS 2000). Proceedings. 2000 IEEE/RSJ International Conference on,* On page(s): 1 - 7 vol.1 Volume: 1, 2000.

Implementation of Taguchi Design for Dry Friction Coefficient of Epoxy Composites

Sudheer M[#1]

[#]*Department of Mechanical Engineering, St. Joseph Engineering College, Mangaluru*
Karnataka-575028, India

`msudheerm2002@yahoo.co.in`

Abstract—**The sliding friction behaviour of 5%, 10% and 15% Potassium Titanate Whiskers (PTW) filled epoxy composites under dry sliding conditions is studied on pin-on-disc configuration. The tests are conducted as per L_{27} orthogonal array of Taguchi design of experiments. Analysis of signal-to-noise (S/N) ratio is carried out to determine optimal combination of test parameters such as sliding velocity (A), normal load (B), filler content (C) and sliding distance (D) for minimizing the frictional performance of developed composites. Analysis of variance (ANOVA) is carried out to identify the contribution of control parameters on the output performance. A multiple regression model is developed to correlate the friction coefficient with control parameters.The present study demonstrated the suitability of Taguchi method for minimizing the frictional performance and optimizing test parameters under dry sliding conditions.**

Keywords— **ANOVA, Ceramic whiskers, Epoxy, Friction coefficient, Taguchi method**

I. INTRODUCTION

Now a days polymer composites reinforced with ceramic fillers are finding extensive applications as non-metallic friction materials [1-4]. A friction coefficient, defined as the ratio of force that resists sliding to the normal force is the primary metric of performance in any tribological system. Friction coefficient can dictate required motor torques and loads, hence is quantified in good number of tribological studies. Many times, friction preferred is to be as low as possible; however, it needs to be moderate some times, as in braking and clamping applications [5]. The primary aim in such applications is to have considerable friction with less wear.

Whiskers are reckoned as more effective reinforcements for polymers and they fall between fibers and particulates. Nearly perfect crystal structure and excellent mechanical properties of these whiskers make them viable alternative for reinforcement with polymers [6]. Potassium titanate whisker (PTW, K_26TiO_{13}) has been found to be a promising reinforcer due to its unique properties, such as outstanding mechanical performance, low hardness (Mohs hardness 4) and excellent chemical stability [7]. Different studies have been reported on frictional behavior of PTW filled polymer composites [8-12].

To date, investigations on the effects of test parameters and material combinations on friction coefficient of ceramic whisker filled thermoset polymers are limited. Therefore, this study attempts to evaluate the sliding friction performance of PTW reinforced epoxy composites under dry sliding conditions. An inexpensive and easy-to-operate Taguchi's technique has been adopted to study effect of various parameters and their interactions on the frictional performance.

II. MATERIALS AND METHODS

A. Materials

Epoxy resin (LY556) with hardener (HY951) was used as the matrix material. Potassium titanate whiskers used as filler material. These whiskers are having high aspect ratio and of splinter (irregular) shape. The morphology of these whiskers is illustrated elsewhere [13].

B. Sample Preparation

Epoxy based composites with different percentages (0-15 wt%) of Potassium Titanate Whiskers (PTW) are prepared using vacuum assisted casting technique.The detailed casting procedure can be referred elsewhere [14].

C. Sliding Friction Testing

The dry sliding friction tests were performed on pin on disc test set up (DUCOM TR 201C) as per ASTM G99-05 standard.The parametersselected are presented in Table 1. Frictional force (N) was directly measured from the friction monitor. The Friction Coefficient (FC) was calculated as per Equation (1).

$$\text{Frictional coeffiient (FC)} = \frac{\text{Tangential frictional force}}{\text{Normal load}} \quad (1)$$

D. Taguchi Experimental Design

The experimental design proposed by Taguchi involves using orthogonal arrays to organize the parameters affecting the process and the levels at which they should be varied; it allows for the collection of the necessary data to determine which factors most affect product quality with a minimum amount of experimentation, thus saving time and resources. Analysis of variance (ANOVA) on the collected data from the Taguchi design of experiments can be used to select new parameter values to optimize the performance characteristic [15].It is well known that the frictional and/or wear performance of polymer composites depends on not only on the material parameters, but also on stress conditions such as normal load, sliding velocity and sliding distance [5]. In the present analysis, filler content as material parameter and test parameters such as applied load, sliding distance and normal load are considered for measuring its influence on the friction. The plan of the experiment [16, 17] is as follows: the first column of the Taguchi orthogonal array is assigned to the sliding velocity (A), the second column to the normal load (B), the fifth column to the fiber content (C), the ninth column to sliding distance (D) and remaining columns are assigned to their interactions and experimental errors.

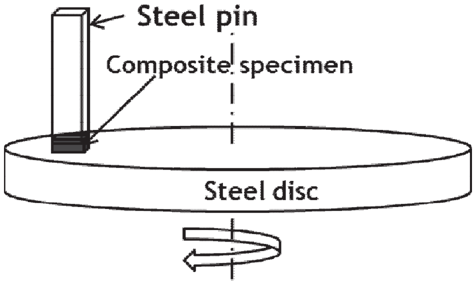

Fig. 1 Dry sliding pin on disc set up.

The S/N ratio is the most important component of parameter design in Taguchi method. The term 'signal' represents the desirable target and the term 'noise' represents the undesirable value. The experimental observations are transformed into signal-to-noise (S/N) ratio. There are several S/N ratios available depending on the type of characteristic, which can be calculated as logarithmic transformation of the loss function. For lower is the better performance characteristic S/N ratio is calculated as per Equation (2).

$$\frac{S}{N} = -10 \log \frac{1}{n} \left(\sum y^2\right) \qquad (2)$$

Where 'n' is the number of observations, and 'y' the observed data. "Lower is the better" (LB) characteristic, with the above S/N ratio transformation, is suitable for minimization of friction coefficient. It is proposed that the quality characteristics are optimized when the S/N response is large as possible. A statistical analysis of variance (ANOVA) is performed to identify the control parameters that are statistically significant. With the S/N ratio and ANOVA analyses, the optimal combination of friction parameters is predicted to acceptable level of accuracy. Finally a confirmation experiment is conducted to verify the optimal process parameters obtained from the parameter design [15].

TABLE I
PROCESS VARIABLES AND THEIR LEVELS

Process variables		**Levels**	
	I	**II**	**III**
A: Sliding velocity (m/s)	0.50	0.75	1.00
B: Normal load (N)	10	20	30
C: Filler content (wt%)	5	10	15
D: Sliding distance (m)	500	1000	1500

E. Regression Analysis

As an attempt to correlate the friction coefficient of composites with the control parameters, a linear regression equation is developed from least squares analysis [18]. The generalized linear regression equation for the experiment can be written as,

$$Y = a_0 + a_1 x_1 + a_2 x_2 + a_3 x_3 + a_4 x_1 x_2 + a_5 x_2 x_3 + a_6 x_3 x_1 \qquad (3)$$

The factorial design of experiments and the values of the response variables corresponding to each set of trials are represented in Equation (3). Here, Y is friction coefficient. The variables x_1, x_2, and x_3 are the control variables used in the experiment. The intercept a_0 refers to the average value of response. The a_1, a_2 and a_3 are the coefficients of the independent variables x_1, x_2 and x_3 respectively. The a_4, a_5, and a_6 are the interaction coefficients between x_1x_2, x_2x_3 and x_1x_3 respectively for the friction coefficient model, with on the selected levels of each variable. Regression model results are compared with the experimental observations.The statistical analysis is made using the software MINITAB 14 specifically used for design of experiment applications.

III. RESULTS AND DISCUSSION

A. Statistical Analysis of Friction Coefficient (FC)

Experimental conditions with friction coefficient results using L_{27} orthogonal array are presented in Table 2. From Table 2, the overall mean for the S/N ratio of friction coefficient is found to be 5.067db. Process parameter settings with the highest S/N ratio always give the optimum quality with minimum variance. The control parameter with the strongest influence is determined by the difference between the maximum and minimum value of the mean of S/N ratios. Higher the difference between the mean of S/N ratios, the more influential is the control parameter [15]. Figure 2 shows graphically the mean of S/N ratios for friction coefficient. The graphs show the change of the S/N ratio when the setting of the control factor is changed from one level to the other. The best friction coefficient is at the higher S/N values in the response graphs. From the plot it is clear that factor combination of A_2, B_3, C_1 and D_1 gives minimum friction coefficient. Thus minimum FC for the developed composites is obtained when sliding velocity (A=0.75m/s) is at intermediate level, normal load (B=30N) is at highest level and filler content (C=5%) and sliding distance (D=500m) are at lowest level.

The S/N ratio responses are given in Table 3, from which it can be concluded that among all the factors, normal load is the most significant factor followed by sliding distance, filler content and sliding velocity. This observation is in line with Equation (1) where it can be noted that friction coefficient is major function of normal load. However, present experimental observations and also the statistical analysis indicated that friction is also the function of whisker content and other test parameters. The less contribution from the filler content and siding velocity on the friction can be attributed to the lower range of values considered for these parameters in the analysis.The factorial design techniques also incorporate the simple means of testing the interaction effects between the control factors. Estimating the interaction between two parameters means checking the non-parallelism of factor effects.

TABLE II
TEST CONDITIONS WITH OUTPUT RESULTS USING L_{27} ORTHOGONAL ARRAY

SI. No	**Sliding Velocity A: (m/s)**	**Normal Load B: (N)**	**Filler Content C: (%)**	**Sliding Distance D: (m)**	**Friction Coefficient (FC)**	**S/N Ratio (dB)**
1	0.50	10	5	500	0.600	4.43697
2	0.50	10	10	1000	0.690	3.22302
3	0.50	10	15	1500	0.780	2.15811
4	0.50	20	5	1000	0.530	5.51448
5	0.50	20	10	1500	0.610	4.29340
6	0.50	20	15	500	0.480	6.37518
7	0.50	30	5	1500	0.570	4.88250
8	0.50	30	10	500	0.430	7.33063
9	0.50	30	15	1000	0.493	6.14306
10	0.75	10	5	1000	0.620	4.15217
11	0.75	10	10	1500	0.730	2.73354
12	0.75	10	15	500	0.630	4.01319
13	0.75	20	5	1500	0.560	5.03624
14	0.75	20	10	500	0.460	6.74484
15	0.75	20	15	1000	0.545	5.27207
16	0.75	30	5	500	0.380	8.40433
17	0.75	30	10	1000	0.453	6.87804
18	0.75	30	15	1500	0.510	5.84860
19	1.00	10	5	1500	0.600	4.43697
20	1.00	10	10	500	0.670	3.47850
21	1.00	10	15	1000	0.785	2.10261
22	1.00	20	5	500	0.535	5.43292
23	1.00	20	10	1000	0.540	5.35212
24	1.00	20	15	1500	0.660	3.60912
25	1.00	30	5	1000	0.493	6.14306
26	1.00	30	10	1500	0.486	6.26727
27	1.00	30	15	500	0.472	6.52116

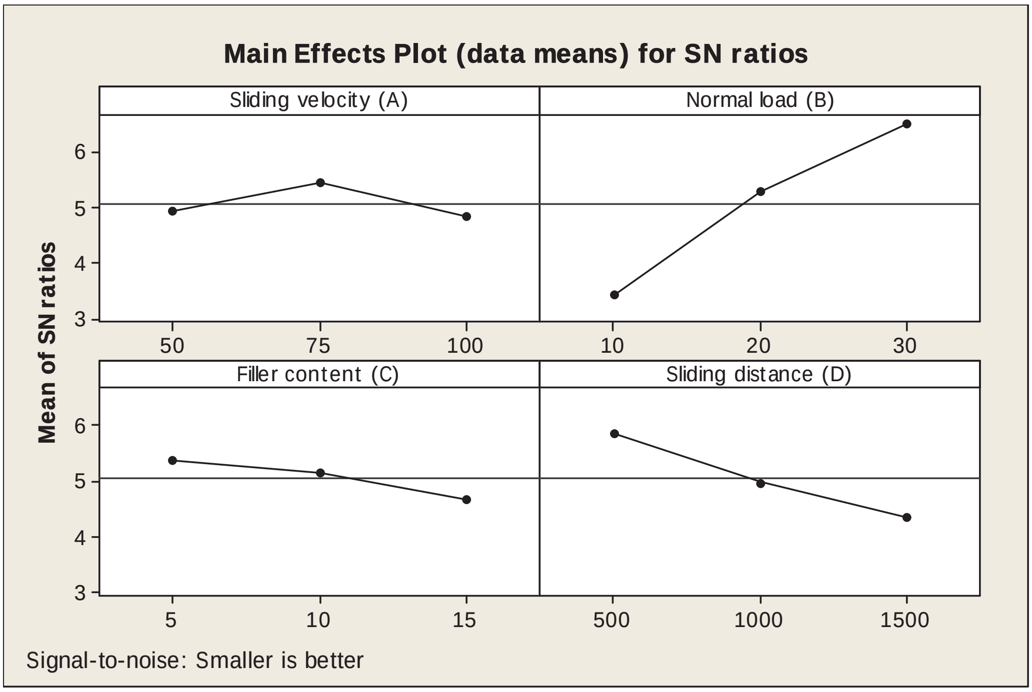

Fig. 2 Effect of control factors on friction coefficient (S/N Ratio).

TABLE III
RESPONSE TABLE FOR SIGNAL TO NOISE RATIOS

Level	**A**	**B**	**C**	**D**
1	4.929	3.415	5.382	5.860
2	5.454	5.292	5.145	4.976
3	4.816	6.491	4.671	4.363
Delta	0.638	3.076	0.711	1.497
Rank	4	1	3	2

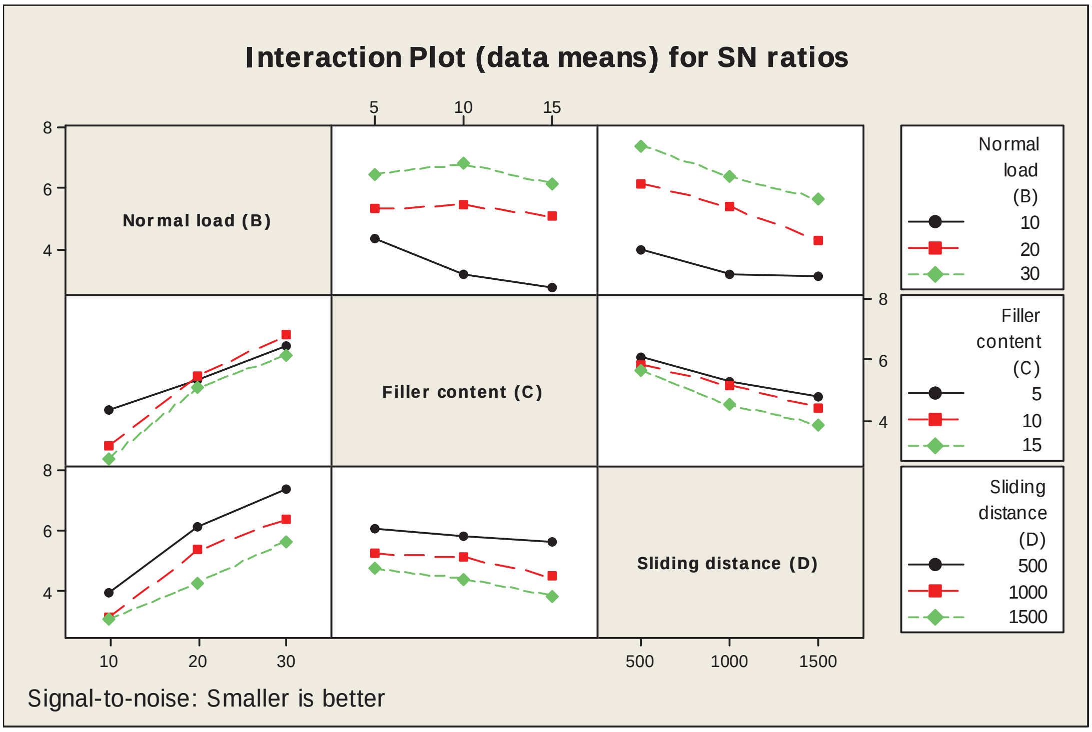

Fig. 3 Interaction graph between B, C and D for friction coefficient (S/N Ratio).

TABLE IV
ANOVA TABLE FOR FRICTION COEFFICIENT

Source	**DOF**	**SS**	**MS**	**F-test**	**p-value**	**P (%)**
Sliding velocity (A)	2	2.0851	1.0426	1.95	0.223	3.20
Normal Load (B)	2	43.2673	21.6337	40.39	0.000	66.42
Filler Content (C)	2	2.3563	1.1782	2.20	0.192	3.61
Sliding distance (D)	2	10.1934	5.0967	9.52	0.014	15.65
(B×C)	4	2.5989	0.6497	1.21	0.396	3.99
(B×D)	4	1.1700	0.2925	0.55	0.709	1.79
(C×D)	4	0.2407	0.0602	0.11	0.974	0.36
Error	6	3.2138	0.5356			4.98
Total	26	65.1256				100

R-Sq = 95.07%   R-Sq (adj) = 78.62%

DOF=Degrees of freedom; SS=Sum of squares; MS=Mean Squares; P=Percentage of contribution.

It is well known that interactions do not occur when lines on the interaction plot are parallel. In other words, if the lines on the interaction graphs are non-parallel, interaction occurs and if the lines cross, strong interaction occurs between factors [15]. Figure 3 illustrates the interaction effects of control parameters. An examination of the Figure 3 yields some interaction between parameter B and C and also between parameter B and D. However, interaction occurring between C×D is little significant. The factor A individually has less contribution on output performance, and their combination of interaction with factor B, C and D (i.e. A×B, A×C and A×D) can be neglected for further study. In order to validate the insignificant factor and insignificant interaction a further statistical analysis (ANOVA) is carried out.

B. ANOVA and Effect of Factors

ANOVA is a statistical design method used to break up the individual effects from all control factors. The percentage contribution of each control factor is employed to measure the corresponding effect on the quality characteristic. Table 4 shows the results of the ANOVA with the friction coefficient. This analysis is undertaken for a level of significance (α) of 5% i.e. for level of confidence 95%. The 7th column of the Table 4 indicates the order of significance among factors and interactions. From Table 4, one can observe that the normal load has greater static influence of 66.42%, sliding distance has an influence of 15.65%, filler content has an influence of 3.61% and sliding velocity has an influence of 3.20% on friction coefficient. Among the interactions, normal load and filler content (p=0.396), normal load and sliding distance (p=0.709) show little effect on friction coefficient and lastly filler content and sliding distance (p=0.974) show neglecting effect on coefficient of friction. The higher R^2 value (95.07%) in the ANOVA results confirms the fit of the model to explain the variability in friction coefficient.

C.Confirmation Experiment

The confirmation experiment is the final step in the design of experiment process. The purpose of the confirmation experiment is to validate the conclusions drawn during the analysis phase. The estimated S/N ratio for friction coefficient using the optimum level of parameters can be calculated with the help of following predictive equation [15]:

$$\bar{\eta}_{opt} = \bar{T} + \sum_{j=1}^{k}\left(\eta_j - \bar{T}\right);\ j = 1,2,\ldots,k. \quad (4)$$

Where, $\bar{T}$= Overall experimental average of S/N ratio.
η_j= mean of the S/N ratio at the optimum parameter level.
k = number of main design parameters that significantly affect the friction coefficient of Epoxy/PTW composites.

The predictive equation for the optimum friction parameters $A_2B_3C_1D_1$ can be written as per Equation (5).

$$\begin{aligned}\bar{\eta}_{opt} = \bar{T} &+ (\overline{A_2} - \bar{T}) + (\overline{B_3} - \bar{T}) + (\overline{C_1} - \bar{T}) + (\overline{D_1} - \bar{T}) \\ &+ [(\overline{B_3C_1} - \bar{T}) - (\overline{B_3} - \bar{T}) - (\overline{C_1} - \bar{T})] \\ &+ [(\overline{B_3D_1} - \bar{T}) - (\overline{B_3} - \bar{T}) - (\overline{D_1} - \bar{T})] \\ &+ [(\overline{C_1D_1} - \bar{T}) - (\overline{C_1} - \bar{T}) - (\overline{D_1} - \bar{T})] \quad (5)\end{aligned}$$

$\overline{A_2}$, $\overline{B_3}$, $\overline{C_1}$ and $\overline{D_1}$= Mean response for factors and interactions at designated levels. By combining the similar terms, Equation (5) reduces to

$$\bar{\eta}_{opt} = \overline{A_2} - \overline{B_3} - \overline{C_1} - \overline{D_1} + \overline{B_3C_1} + \overline{B_3D_1} + \overline{C_1D_1} \quad (6)$$

The results of experimental confirmation using optimal friction parameters and comparison of the predicted friction coefficient with the actual friction coefficient using the optimal friction parameters are shown in Table 5. Good agreement seems to take place between the estimated and actual friction coefficient. The improvement in S/N ratio from the starting level to optimum level is 4.11 dB. The friction coefficient is reduced by 37.70%. Therefore the frictional performance is considerably improved by using Taguchi method.

D. Linear Regression Model

A multiple linear regression analysis attempts to model the relationship between two or more predictor variables and a response variable by fitting a linear equation to the observed data [18]. In order to establish the correlation between the test parameters (i) sliding speed (ii) normal load (iii) filler content (iv) sliding distance and the friction coefficient, a multiple linear regression model is generated using the MINITAB computer program and is presented in Equation (7). The large value of R^2 indicates that 87.4% of variation in friction coefficient is explained by developed regression model which can be considered as good estimate.

$$\begin{aligned}\text{Friction Coefficient (FC)} &= 0.575 + 0.000129\times A \\ &- 0.00562\times B + 0.0115\times C + 0.000019\times D \\ &- 0.000572\times B\times C + 0.000001\times B\times D + 0.000005\times C\times D \quad (7)\end{aligned}$$

Coefficient of determination R^2 = 87.4%

The coefficient associated with load (B) in the regression Equation (7) is negative and it indicates that as the load increases, friction coefficient of the composite decreases. Whereas friction coefficient increases with sliding velocity (A), filler content (C) and sliding distance (D). These effects are also confirmed by Taguchi method.

TABLE V
CONFIRMATION TEST FOR FRICTION COEFFICIENT

	Initial process parameters	**Optimal process parameters**		**Improvement in the result**
		Prediction	Experimental	
Level	$A_1B_2C_3D_3$	$A_2B_3C_1D_1$	$A_2B_3C_1D_1$	
S/N ratio (dB)	4.2934	7.7075	8.4043	4.11 dB
Friction coefficient	0.610	0.419	0.380	37.70 %

When the measured values of the variables are substituted in Equation (7), friction coefficient of the composites could be calculated within the range of the factors investigated. Table 6 shows the results obtained where comparison is carried out between the foreseen values from the regression model developed in the present work (Equation 7), with the values obtained experimentally. From the analysis of the referred table one can observe that the calculated error varies from 3.78% to 7.47% for friction coefficient. Therefore the multiple regression equation derived above correlate the evaluation of the friction coefficient of the composites with the reasonable degree of approximation.

TABLE VI
CORRELATION BETWEEN EXPERIMENTAL VALUES AND REGRESSION MODEL RESULTS

Test	Parameters	Experimental Value	Regression model (Eq.(7))	Percentage Error
1	$A_1B_2C_3D_3$	0.610	0.64095	4.83
2	$A_2B_1C_2D_2$	0.640	0.66520	3.78
3	$A_3B_3C_1D_1$	0.460	0.42800	7.47

IV. CONCLUSIONS

Taguchi's robust design method is used to analyse the dry sliding frictional behaviour of the ceramic whisker filled polymer matrix composites as described in the paper. The following are broad conclusions that can be drawn from the work.

1. Design of experiment approach by Taguchi method enable us to analyse successfully the frictional behaviour of composites with the sliding velocity, normal load, filler content and sliding distance as test variables. From the S/N ratio analysis, the optimal combination of friction parameters is obtained as $A_2B_3C_1D_1$ to minimize friction coefficient.
2. ANOVA results indicated that normal load is the factor which is having highest statistical influence on the friction coefficient of the composites (66.42%) followed by sliding distance (15.65%), filler content (3.61%) and sliding velocity (3.20%). However interaction of these factors shows less significant effect on friction coefficient.
3. The confirmation tests indicated that it is possible to decrease friction coefficient significantly (37.70%) by using the proposed statistical technique. The experimental results confirmed the validity of Taguchi method for enhancing the frictional performance and optimizing the control parameters under dry friction conditions.
4. A comparison between the experimental values and multiple regression model results for friction coefficient of the composites indicated an error of 3.78% to 7.47%. Thus regression model results effectively correlate with the experimental values.

In future, this study can be extended to learn the frictional behaviour of similar multiphase polymer composites.

ACKNOWLEDGMENT

Author remains grateful to Director, Principal, and Vice-Principal and Head of Mechanical Engineering of St. Joseph Engineering College, Mangaluru, Karnataka, India fortheir support to carry out this work.

REFERENCES

[1] D. Chan and G. W. Stachowiak, "Review of automotive brake frictional material", *Proceedings of Institution of Mechanical Engineers, Part D: Journal of Automobile Engineering* 218, pp. 953-966, 2004.

[2] Y.C. Kim, M.H. Cho, S.J. Kim and H. Jang, "The effect of phenolic resin, potassium titanate, and CNSL on the tribological properties of brake friction materials", *Wear* 264, pp. 204–210, 2008.

[3] N.Dadkar, B.S. Tomar and B.K. Satapathy, "Evaluation of flyash-filled and aramid fibre reinforced hybrid polymer matrix composites (PMC) for friction braking applications", *Materials and Design* 30,pp. 4369-4376, 2009.

[4] Y. Ma, G.S.Martynkova, M. Valaskova, V.Matejka and Y. Lu "Effects of $ZrSiO_4$ in non-metallic brake friction materials on friction performance", *Tribology International* 41(3), pp. 166-174, 2008.

[5] G.W. Stachowiak and A.W. Batchelor, *Engineering tribology*, 2ndEditon, Butterworth-Heinemann:Oxford, 2001.

[6] V.M. Johnand S.K. Harry, *Whiskers, In: Handbook of Reinforcements for Plastics,* Van Nostrand Reinhold, New York, pp. 205-229, 1987.

[7] T. Zaremba and D. Witkowska, "Methods of manufacturing of potassium titanatefibres and whiskers. A review," *Materials Science- Poland* 28(1), pp. 25–41, 2010.

[8] S.J. Kim, M.H. Cho, R.H. Basch, J.W. Fash and H. Jang, "Tribological properties of polymer composites containing barite ($BaSO_4$) or potassium titanate ($K_2O.6(TiO_2)$)", *Tribology Letters* 17(3), pp. 655-661, 2004.

[9] G.Y. Xie, G.S. Zhuang, G.X. Sui and R. Yang, "Tribological behavior of PEEK/PTFE composites reinforced with potassium titanate whiskers", *Wear* 268, pp. 424–430, 2010.

[10] G. Zhao, T. Wang and Q. Wang, "Friction and wear behavior of the polyurethane composites reinforced with potassium titanate whiskers under dry sliding and water lubrication", *Journal of Materials Science* 46, pp. 6673–6681, 2011.

[11] Y.J. Shi, X. Feng, H.Y. Wang, C. Liu and X.H. Lu, "Effects of filler crystal structure and shape on the tribological properties of PTFE composites", *Tribology International* 40, pp. 1195–1203, 2007.

[12] Z. Zhu, L. Xu and G. Chen, Effect of different whiskers on the physical and tribological properties of non-metallic friction materials, *Materials and Design* 32, 2011, pp. 54–61.

[13] M. Sudheer, K. Sandesh, K. Raju and ThirumaleshwaraBhat, "Abrasive wear performance of epoxy/glass/PTW composites", *Annual Research Journal, NMAM Institute of Technology*, Volume 3, pp. 36-42, 2013.

[14] M. Sudheer, RavikanthaPrabhu, K. Raju, ThirumaleshwaraBhat, "Optimization of dry sliding wear performance of ceramic whisker filled epoxy composites using Taguchi approach", *Advances in Tribology*, Volume 2012, Article ID 431903, pp. 1-9, 2012.

[15] K.R. Ranjit, *A Primer on the Taguchi Method*, Van Nostrand Reinhold, New York, 1990.

[16] Siddhartha, A. Patnaik and A.D. Bhatt, "Mechanical and dry sliding wear characterization of epoxy-TiO_2 particulate filled functionally graded composite materials using Taguchi design of experiment", *Materials and Design* 32, pp. 615-627, 2011.

[17] Rashmi, N.M. Renukappa, B. Suresha, R.M. Devarajaiah and K.N. Shivakumar, "Dry sliding wear behaviour of organo-modified montmorillonite filled epoxy nanocomposites using Taguchi's techniques", *Materials and Design* 32, pp. 4528-4536, 2011.

[18] D.C. Montgomery, G.C. Runger. *Applied Statistics and Probability for Engineers*, 2nd Edition, John Wiley & Sons Inc, New York, 1999.

Anti-aliasing Lifting Scheme for Gear Fault Diagnosis

B Vishwash[#1], Srinivasa Pai P[#2], Vijay G S[*3]

[#]*Department of Mechanical Engineering, NMAMIT, Nitte, Udupi-574 110, India*
**Department of Mechanical and Manufacturing Engineering, MIT, Manipal University, Manipal-576 104, India*

[*]`srinivasapai@rediffmail.com`

Abstract— **In this paper fault diagnosis of gear has been done using three Lifting Schemes namely the conventional Lifting Scheme, Redundant Lifting Scheme and Anti-aliasing Lifting Scheme. In the Anti-aliasing Lifting Scheme the frequency aliasing occurring in other two schemes is avoided. The vibration signals acquired from gears have been used for fault feature extraction using these lifting schemes to differentiate between two conditions of gear. The extracted features have been evaluated using Multilayer Perceptron Neural Network (MLPNN) to compare the effectiveness of the three Lifting Schemes. The prediction accuracies obtained on test data using MLPNN has shown that the Anti-aliasing Lifting Scheme is effective for fault diagnosis of gear when compared to the conventional Lifting Scheme and Redundant Lifting Scheme.**

Keywords— **Vibration based Condition Monitoring, Fault Diagnosis, Lifting Scheme, Redundant Lifting Scheme, Anti-aliasing Lifting Scheme and Multilayer Perceptron Neural Network.**

I. INTRODUCTION

Gears are critical mechanical components in many mechanical systems, the failure of which may lead to small damages to mechanical system or a serious accident leading to the destruction of entire system and sometimes may even harm surrounding machineries and machine operators. The failure may also lead to severe economic losses [1].

Fault diagnosis is necessary not only for guaranteeing the safe run of machines but is also necessary for achieving economical maintenance [1, 2]. Vibration signals have played a significant role for fault diagnosis in many industrial applications as they are accurate in many cases thus proving their effectiveness in preventing any downtime of machineries and guaranteeing the normal running of machines [2, 3]. And it is found that the vibrational signals can capture dominant information about the machine elements which is very much desirable for the fault diagnosis of mechanical systems [1-3]. In many cases the noise present in the measured vibration signals will bury the important information about the condition of machine [3].

Denoising the signals will help in removing the noise from the signals. The denoised vibration signals can be used for fault feature extraction. It is evident from literature that Wavelet Transform has been used widely for feature extraction from vibration signals. But it has a drawback in choosing the appropriate mother wavelet or also to design wavelets for desired application. [1-4]. To avoid such difficulties for fault feature extraction from denoised vibration signals for fault diagnosis of gears, many researchers have adopted Lifting Scheme [4, 5] and Redundant Lifting Scheme [6, 7]. But there exists frequency aliasing in these two Lifting Schemes. To overcome this frequency aliasing, an improved Lifting Scheme known as Anti-aliasing Lifting Scheme has been proposed by Bao et. al as described in [8].

In this study all the three Lifting Schemes have been investigated for fault diagnosis of gear. The Lifting Scheme of the Daubechies Wavelet of order 8 (db8) that forms the second generation wavelet [8] has also been used for fault diagnosis of gear.

The extracted features using these Lifting Schemes from denoised vibration signals have been evaluated using Artificial Neural Network (ANN). MLPNN, one of the most widely used ANN model has been used for evaluation [9]. Further to evaluate the effectiveness of Anti-aliasing Lifting Scheme envelope spectrum computed using Low Pass Filter (LPF) and Hilbert Transform (HT) has been used [8].

The paper is organized as follows. Section 1 presents the introduction, section 2 presents the overview of the Lifting Schemes, section 3 gives introduction to ANN, section 4 describes the experimental data, section 5 presents the feature extraction based on Lifting Schemes and evaluation using ANN, section 6 presents the Lifting Scheme applied to Daubechies Wavelet, section 7 presents the comparison of Lifting Scheme and Anti-aliasing Lifting Scheme and finally section 8 gives the conclusion.

II. OVERVIEW OF LIFTING SCHEMES

The Lifting Scheme was first introduced by Wim Sweldens in 1998 which is the conventional Lifting Scheme. The improved version of the Lifting Scheme is Redundant Lifting Scheme and Anti-aliasing Lifting Scheme which is the latest improved model of the Lifting Scheme [8]. The following sections describe these schemes.

A. *Lifting Scheme*

The lifting scheme was introduced to adjust the wavelet transform to irregular sampling and complex geometries which gave rise to second-generation wavelet transform [4]. The main features of the Lifting Scheme include easy to understand and implement, to replace the original signal with its wavelet transform, and ability requirement for less computations when compared to Continuous Wavelet Transform (CWT) and Discrete Wavelet Transform (DWT) by allowing faster execution of the wavelet transform [5].

The Lifting Scheme consists of three steps namely split, prediction and update [8]. In the split step, the input samples a_l are split as even subset of samples a_{l-1} and odd subset of samples d_{l-1} as shown in (1). In the prediction step the even set of samples are used to predict the odd set of samples as shown in (2). The update operator gives improved even set of samples by retaining the resolution of the input samples as shown in (3) [4, 8].

$$\{a_{l-1}, d_{l-1}\} = S(a_l) \tag{1}$$

$$d_{l-1} = d_{l-1} - P(a_{l-1}) \tag{2}$$

$$a_{l-1} = a_{l-1} + U(d_{l-1}) \tag{3}$$

$$P = [p(0),......., p(M-1)] \tag{4}$$

$$U = [u(0),......, u(N-1)] \tag{5}$$

where P and U are prediction and update operators and M and N are their lengths respectively. After executing all the three decomposition steps a_{l-1} represents approximate coefficients and d_{l-1} represents detail coefficients. The reconstruction steps of the Lifting Scheme includes inverse update, inverse prediction and merge which are shown in (6), (7) and (8) respectively [5, 8].

$$a_{l-1} = a_{l-1} - U(d_{l-1}) \tag{6}$$

$$d_{l-1} = d_{l-1} + P(a_{l-1}) \tag{7}$$

$$a_l = M(a_{l-1}, d_{l-1}) \tag{8}$$

Fig. 1 shows the decomposition and reconstruction procedure of Lifting Scheme. But in the Lifting Scheme, the frequency aliasing is caused in the split and merge operations as the Sampling Theorem cannot be satisfied [7, 8]. To overcome this problem improved version of Lifting Scheme known as Redundant Lifting Scheme was proposed [6-8].

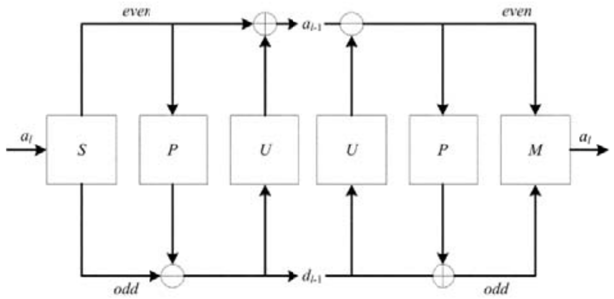

Fig. 1 Decomposition and reconstruction procedure of the Lifting Scheme

B. *Redundant Lifting Scheme*

In the Redundant Lifting Scheme split and merge operations are removed to avoid frequency aliasing caused in Lifting Scheme [6]. But since the split and merge steps are eliminated the prediction operator P and update operator U are modified to P^l and U^l to obtain prediction coefficients and update coefficients as shown in (9) and (10) [6, 8].

$$p_i^l = p_0^0, \underbrace{0,...0}_{2^l-1}, p_1^0, \underbrace{0,...0}_{2^l-1}, p_2^0, ..., p_{M-2}^0 \underbrace{0,...0}_{2^l-1}, p_{M-1}^0 \tag{9}$$

$$u_i^l = u_0^0, \underbrace{0,...0}_{2^l-1}, u_1^0, \underbrace{0,...0}_{2^l-1}, u_2^0, ..., u_{N-2}^0 \underbrace{0,...0}_{2^l-1}, u_{N-1}^0 \tag{10}$$

The detail coefficients d_{l-1} and approximate coefficients a_{l-1} obtained from signal X using Redundant Lifting Scheme at level l are shown in (11) and (12) [6-8].

$$d_{l-1} = X - P^l X \tag{11}$$

$$a_{l-1} = X + U^l d_{l-1} \tag{12}$$

In the Redundant Lifting Scheme the frequency aliasing caused by split and merge operations have been removed but still there exists a frequency aliasing in prediction and update steps and its inverse. Therefore the improved version of the Redundant Lifting Scheme know as Anti-aliasing Lifting Scheme was introduced [8]

C. *Anti-aliasing Lifting Scheme*

To remove the frequency aliasing occurring in prediction and update operators due to unideal frequency, the two operators namely CA and CD known as anti-aliasing operators for integrated input signal $x(n)$ with length N at level l were introduced as shown in (13) and (14) respectively [8].

$$\overline{X}(k) = \sum_{n=0}^{N-1} x(n) W^{kn}, 0 \le k \le \frac{N}{2^{l+1}}, \frac{(2^{l+1}-1)N}{2^{l+1}} \le k \le N$$
$$\overline{X}(k) = 0, \text{otherwise} \tag{13}$$
$$\overline{X}_a(n) = \frac{1}{N} \sum_{n=0}^{N-1} \overline{X}(k) W^{-kn},$$

$$\overline{X}(k) = \sum_{n=0}^{N-1} x(n) W^{kn}, \frac{N}{2^{l+1}} \le k \le \frac{N}{2^l}, \frac{(2^l-1)N}{2^l} \le k \le \frac{(2^{l+1}-1)N}{2^{l+1}}$$
$$\overline{X}(k) = 0, \text{otherwise} \tag{14}$$
$$\overline{X}_d(n) = \frac{1}{N} \sum_{n=0}^{N-1} \overline{X}(k) W^{-kn}$$

where $\overline{X}_a(n)$ and $\overline{X}_d(n)$ are outputs of CA and CD respectively [8]. Fig. 2 shows the decomposition procedure of the Anti-aliasing Lifting Scheme, Fig. 3 shows the single subband reconstruction for approximation of the Anti-aliasing

Lifting Scheme and Fig. 4 shows the single subband reconstruction for detail of the Anti-aliasing Lifting Scheme [8].

In this way the frequency aliasing has been completely removed in Anti-aliasing Lifting Scheme in which the split and merge operations are removed and the anti-aliasing operators CA and CD are added when compared to the conventional Lifting Scheme [8]. To remove redundant frequency components first the fast Fourier transform (FFT) should be applied to intergraded signals and redundant frequencies should be left to zero, then inverse fast Fourier transform is applied to the resultant spectra [8].

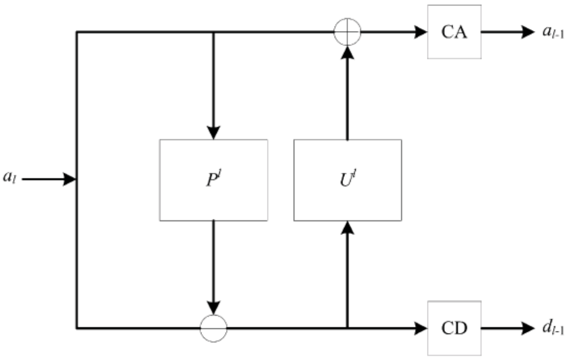

Fig. 2 Decomposition procedure of the Anti-aliasing Lifting Scheme

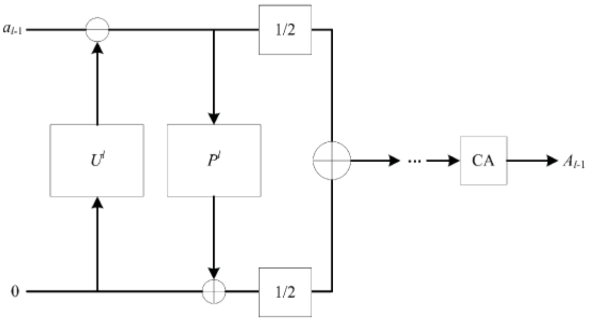

Fig. 3 Single subband reconstruction for approximation of the Anti-aliasing Lifting Scheme

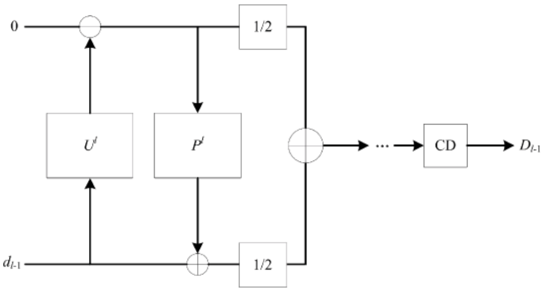

Fig. 4 Single subband reconstruction for detail of the Anti-aliasing Lifting Scheme

III. INTRODUCTION TO ARTIFICIAL NEURAL NETWORK

An artificial neural network (ANN) is defined as a nonlinear mapping tool that relates a set of inputs to a set of outputs. ANN mimics biological neurons by simulating some of the functions of the human brain [9]. An ANN is made up of processing elements called neurons that are interconnected in a network. The artificial neurons receive inputs that are analogous to the electro-chemical signals that natural neurons receive from other neurons. By changing the weights given to these signals, the network learns in a process that seems similar to that found in nature. i.e., neurons in ANN receive signals or information from other neurons or external sources, perform transformations on the signals, and then pass those signals on to other neurons. The way information is processed and stored depends on the architecture and algorithms of ANN [10].

The types of ANNs include Multi-Layer Perceptron neural network (MLPNN), Radial Basis function (RBF) network, Probabilistic Neural Networks (PNN), etc. The most popular neural network is the MLPNN, which is a feedforward network and frequently employed in fault diagnosis systems, which has found immense popularity in condition monitoring applications as it constitutes more than 90% of the current ANN applications [9, 10]. Therefore in this study MLPNN has been used for evaluating features extracted from different Lifting Schemes.

A. MLPNN

MLP network consists of an input layer of source nodes, one or more hidden layers of computation nodes and an output layer. The commonly used structure of the MLP neural network consists of three layers: input layer of source nodes, one or more hidden layers and an output layer. Fig. 5 shows the general MLP structure. Each layer is comprised of nodes $\geqslant 1$ and each node in any layer is connected to all the nodes in the neighbouring layers. These connections have their individual weights which are called synaptic weights and are multiplied to the node values of the previous layer. Input and output data dimensions of the MLPNN determine the number of nodes in the input and output layers, respectively, but the number of hidden layers and their nodes is determined heuristically. The number of hidden layers and nodes in an MLP is proportional to its classification power [9, 10].

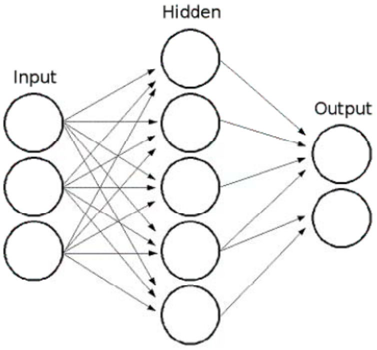

Fig. 5 General MLP Structure

After setting the structure of the MLP, the ANN trained by adjusting the synaptic weights in a way that any particular input leads to the desired output. It can be conducted by different algorithms. For any learning algorithm, a limit should be defined to stop the learning process, which is called Stopping Criterion which is based on one of the three rules or all three rules simultaneously namely, the root mean square error in an epoch becomes less than a predefined value, the error gradient becomes less than a predefined value and the number of epochs reaches a predefined number [9]. The error vector for an MLP is defined as the difference between the network output vector and the desired output vector. Modelling of MLPNN involves selecting an appropriate structure, initial weights, training algorithm for an MLPNN and supplying it with enough training datasets which enables the MLPNN to operate as a powerful classifier [9, 10].

IV. EXPERIMENTAL DATA

The vibration signal data of gears obtained from the experiments conducted by the PHM society [11] using the gear test rig shown in Fig. 6 has been used in this study.

A. Gear Data

The experiments were conducted on the gearbox under 2 different loads, 4 different speeds and using two gear conditions namely spur 1 and spur 5 which are good and defective gears respectively. The vibration signals were acquired using Endevco 6259M31 accelerometers mounted on input and output shafts with input shaft speeds being 30 Hz, 35 Hz, 40 Hz and 45 Hz under low and high loading.

The sampling frequency is 66.6667 kHz. Data has been provided in .mat and .csv files, with three columns – the first column being input voltage, second being output voltage and the third being tachometer readings. The second column which consisted of 266665 data samples and which was reshaped to 260000 data samples have been selected for vibration signal analysis for monitoring the condition of gear for all speeds and loads. The 260000 data samples were divided into 52 bins with each bin containing 5000 data samples [12].

Fig. 6 Photograph of the Gear test rig

V. DENOISING

Raw gear vibration signals acquired at different speeds and loads were denoised before being used for feature extraction using different Lifting Schemes.

For denoising raw vibration signals from gear Daubechies wavelet of order 8 has been used as the mother wavelet which has been decomposed to 4 levels. Hard thresholding with universal threshold as threshold selection rule and multiplicative threshold rescaling has been done using level-dependent estimation of noise level which gave best denoised signal. The denoised vibration signals at different speeds and loads for both spur 1 and spur 5 have been used for extracting features using different Lifting Schemes [12].

VI. FEATURE EXTRACTION AND EVALUATION USING ANN

The statistical features namely peak value, mean, standard deviation, root mean square, shape factor, skewness, kurtosis and crest factor [8] have been extracted from denoised gear vibration signals using all the three Lifting Schemes. The extracted features have been evaluated using MLPNN classifier.

A. Lifting Scheme

The denoised vibration signals have been subjected to split operation. Then the split signals are subjected to prediction and update operations with prediction and update operators being [-0.0625, 0.5625, 0.5625, -0.0625] and [-0.0313, 0.2813, 0.2813, -0.0313] respectively. The signals obtained after update operation have been decomposed to three levels. Then the above mentioned eight statistical features have been extracted from detail coefficients at all three levels and from approximate coefficients at third level. Thus 32 features have been obtained from each bin.

There are 52 bins for one condition of gear at one speed and load. Therefore, in case of four speeds, two loads and two conditions a feature set having 832 patterns is obtained each having 32 features i.e. (32 X 832). The feature set obtained from gear vibration signals were used to train MLPNN with 80% of data being used for training the model and remaining 20 % for testing the model. The prediction accuracy on test data for Lifting Scheme is shown in Table 1.

B. Redundant Lifting Scheme

In Redundant Lifting Scheme the denoised vibration signals have not been subjected to split operation. Instead the denoised signals are directly subjected to prediction and update operations with prediction and update operators being [-0.0625, 0.5625, 0.5625, -0.0625] and [-0.0313, 0.2813, 0.2813, -0.0313] respectively at level zero. The signals obtained after update operation of Redundant Lifting scheme have been decomposed to three levels to extract eight statistical features from detail coefficients at all three levels and from approximate coefficients at the third level. Again 32 features have been obtained from each bin. Therefore, as explained in Lifting Scheme for gear vibration signals a feature set of (32 X 832) have been obtained which were fed to MLPNN. The prediction accuracy on test data for Redundant Lifting Scheme is shown in Table 2.

C. Anti-aliasing Lifting Scheme

Here to remove the frequency aliasing completely the split operation has been removed and the denoised vibration signals were directly subjected to prediction and update operations with prediction and update operators being [-0.0625, 0.5625, 0.5625, -0.0625] and [-0.0313, 0.2813, 0.2813, -0.0313] respectively at level zero. On the processed signals obtained from the update operator the Fast Fourier Transform (FFT) is applied and then the inverse FFT is applied after which the signals have been decomposed into three levels. A feature set of (32 X 832) have been obtained using the Anti-aliasing Lifting Scheme which were fed to MLPNN for training and testing the model. The prediction accuracy on test data for Anti-aliasing Lifting Scheme is shown in Table 3. Table 4 gives the sample output results of test data for Anti-aliasing Lifting Scheme.

VII. Lifting Scheme Applied to Daubechies Wavelet

In the conventional Lifting Scheme, the split operation is performed using a wavelet known as Lazy wavelet. But in the current work Daubechies wavelet of order 8 (db8) has been used and the prediction and operators remain the same. The features extracted from this were fed to MLPNN which gave a classification accuracy of 100% both on training and test data for 20 neurons with an error of 0.0002 and the number of epochs being 1000.

TABLE I
Prediction accuracy on test data for Lifting Scheme

Number of Neurons	**Learning Rate (LR)**	**Momentum Rate (MR)**	**Accuracy on Training data (%)**	**Accuracy on Test data (%)**
5, 10	0.2	0.0001	93.54	93.97
5, 10, 15, 20, 25, 30	0.3	0.0001	49.69	51.20
5, 10, 15, 20, 25, 30	0.4	0.0001	49.69	51.20
5	0.5	0.0001	0	0
10	0.1	0.0001	90.69	90.36
20	0.1	0.0002	90.54	90.36
5	0.1	0.0003	89.78	89.75
10	**0.1**	**0.0004**	**91.14**	**90.96**

TABLE II
Prediction accuracy on test data for Redundant Lifting Scheme

Number of Neurons	**Learning Rate (LR)**	**Momentum Rate (MR)**	**Accuracy on Training data (%)**	**Accuracy on Test data (%)**
5	0.2	0.0001	95.49	94.57
5, 10, 15, 20, 25, 30	0.3	0.0001	49.69	51.20
5, 10, 15, 20, 25, 30	0.4	0.0001	49.69	51.20
5	0.5	0.0001	0	0
15	0.1	0.0001	92.94	96.38
15	0.1	0.0002	92.79	95.78
20	**0.1**	**0.0003**	**92.94**	**92.77**
20	0.1	0.0004	93.84	95.78

TABLE III
Prediction accuracy on test data for Anti-aliasing Lifting Scheme

Number of Neurons	**Learning Rate (LR)**	**Momentum Rate (MR)**	**Accuracy on Training data (%)**	**Accuracy on Test data (%)**
5	0.04	0.001	95.94	95.78
10	0.05	0.001	95.34	96.38
20	**0.05**	**0.001**	**95.94**	**95.78**
30	0.03	0.001	50.30	48.79
15	0.03	0.002	0	0
15	0.03	0.003	5030	48.79

VIII. COMPARISON

It can be seen from the results of the MLPNN that all the three schemes namely Lifting Scheme, Redundant Lifting Scheme and Anti-aliasing Lifting Scheme gave a maximum classification accuracy of 90.96 %, 92.77 % and 95.78 % respectively on test data. The frequency aliasing occurring in Lifting Scheme and Redundant Lifting Scheme has been completely removed in Anti-aliasing Lifting Scheme which improves the performance of the features extracted from the vibration signals. The MLPNN performance on the test data has established this with a highest prediction accuracy of 95.78% on features extracted using Anti-aliasing Lifting Scheme. Further the envelope spectrum of the processed vibration signals obtained from conventional Lifting Scheme and Anti-aliasing Lifting Scheme have been compared. The gear mesh frequency (GMF) of a gear (48Teeth) in the gearbox is 480 Hz.

TABLE IV
Sample output results of test data for Anti-aliasing Lifting Scheme

Target Output		**Network Output**	
1	0	0.967067	0.032933
0	1	0.007806	1.017637
1	0	1.008783	-0.00682
1	0	1.009537	-0.00219
0	1	0.001354	1.001422
0	1	-0.00289	1.023136
1	0	1.006742	-0.00155
0	1	-0.00203	1.012061

The envelope spectrum is shown in Fig. 7 and 8 obtained using Low Pass Filter (LPF) and Hilbert Transform (HT) for Lifting Scheme and Fig. 9 and 10 shows the same using Anti-aliasing Lifting Scheme. It is clear that in the beginning the GMFs can be identified easily, but its multiples have almost died out. And the reason for diminishing of the multiples of GMFs is the frequency aliasing. Since frequency aliasing is completely removed in Anti-aliasing Lifting Scheme the multiples of GMFs can be easily identified in the envelope spectrum as shown in Fig. 9 and 10.

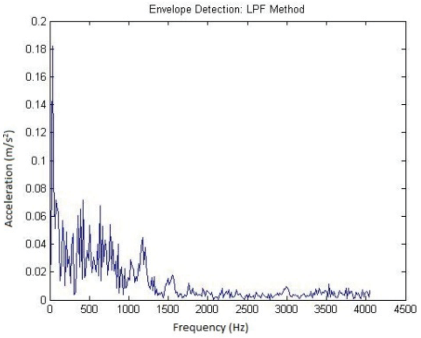

Fig. 7 Envelope spectrum using LPF for Lifting Scheme

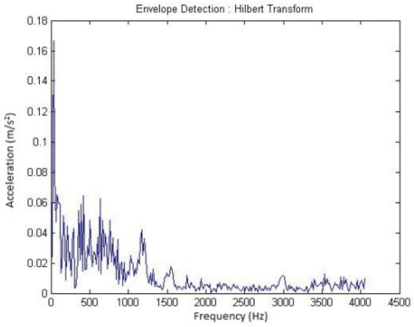

Fig. 8 Envelope spectrum using HT for Lifting Scheme

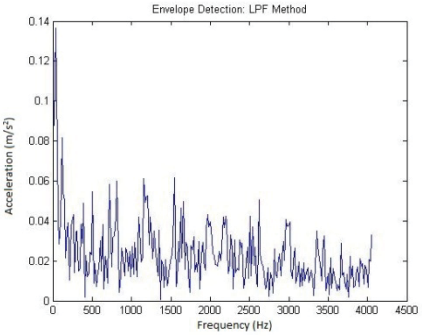

Fig. 9 Envelope spectrum using LPF for Anti-aliasing Lifting Scheme

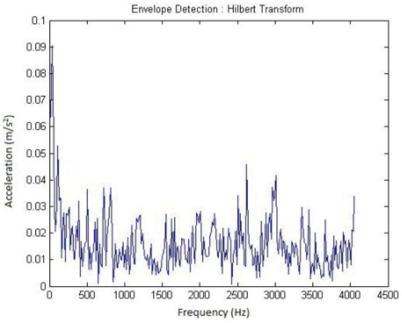

Fig. 10 Envelope spectrum using HT for Anti-aliasing Lifting Scheme

IX. CONCLUSIONS

The features extracted from Lifting Scheme, Redundant Lifting Scheme and Anti-aliasing Scheme have been able to classify different conditions of gear with classification accuracies of 90.96 %, 92.77 % and 95.78 % respectively on test data. From the classification accuracies and the envelope spectrum it can be concluded that the frequency aliasing occurring in Lifting Schemes have been removed completely in Anti-aliasing Lifting Scheme. Therefore the Anti-aliasing Lifting Scheme is effective for the fault diagnosis of gear.

REFERENCES

[1] J. Rafiee, F. Arvani, A. Harifi, M.H. Sadeghi, "Intelligent condition monitoring of a gearbox using artificial neural network", *Mechanical Systems and Signal Processing*, Vol.21, 2007, pp. 1746-1754.

[2] Z.K. Peng, F.L. Chu, "Application of the wavelet transform in machine condition monitoring and fault diagnostics: a review with bibliography", *Mechanical Systems and Signal Processing*, Vol.18, 2004, pp. 199-221.

[3] Zhen Li, Zhengjia He, Yanyang Zi, Hongkai Jiang, "Rotating machinery fault diagnosis using signal-adapted lifting scheme", *Mechanical Systems and Signal Processing*, Vol.22, 2008, pp. 542-556.

[4] Duan Chendong, He Zhengjia, Jiang Hongkai, "A sliding window feature extraction method for rotating", *Journal of Sound and Vibration*, Vol.299, 2007, pp. 774-785.

[5] H.X. Chen, Patrick S.K. Chua, G.H. Lim, "Vibration analysis with lifting scheme and generalized cross validation in fault diagnosis of water hydraulic system", *Journal of Sound and Vibration*, Vol.301, 2007, pp. 458-480.

[6] Jiang Hongkai, He Zhengjia, Duan Chendong, Chen Peng, "Gearbox fault diagnosis using adaptive redundant Lifting Scheme", *Mechanical Systems and Signal Processing*, Vol.20, 2006, pp. 1992-2006.

[7] ZHOU Rui, BAO Wen, ZUO Guo-hua, YU Da-ren, YANG Jian-guo, "Turbine Vibration Fault Feature Extraction Based on Improved Redundant Lifting Scheme", *Proceedings of the CSEE*, Vol.28, 2008, pp. 88-93.

[8] Wen Bao, Rui Zhou, Jianguo Yang, Daren Yu, Ning Li, "Anti-aliasing lifting scheme for mechanical vibration fault feature extraction", *Mechanical Systems and Signal Processing*, Vol.23, 2009, pp. 1458-1473.

[9] A. Hajnayeb, A. Ghasemloonia, S.E. Khadem, M.H. Moradi, "Application and comparison of an ANN-based feature selection method and the genetic algorithm in gearbox fault diagnosis", *Expert Systems with Applications,* Vol.38, 2011, pp. 10205-10209.

[10] Yaguo Lei, Ming J. Zuo, Zhengjia He, Yanyang Zi, "A multidimensional hybrid intelligent method for gear fault diagnosis", *Expert Systems with Applications*, Vol.37, 2010, pp. 1419-1430.

[11] http://www.phmsociety.org/competition/09

[12] B Vishwash, "Fault Diagnosis of Gear Using Vibration Monitoring with Artificial Neural Network (Ann) – A Comparison of Feature Extraction Techniques," ***M. Tech.*** *thesis, Nitte Mahalinga Adyantaya Memorial Institute Technology (NMAMIT)*, Nitte - 574 110, Udupi, Karnataka, India, May 2014.

GUIDELINES FOR AUTHORS

The contributors are expected to highlight their research work with sufficient details & discussion of results.

The original research paper should be limited to 6 and short communication to 3 printed pages of the journal in double column standard IEEE format. Please refer to IEEE website for the standard format.

Manuscripts must be submitted online to nmamit.arj@gmail.com in .docx format.

Enough precaution should be taken to make the manuscript error free.

The papers that are not in the standard format may be rejected

Submission of an article implies that the work described has not been published previously (except in the form of an abstract or as part of a published lecture or academic thesis), that it is not under consideration for publication elsewhere, that its publication is approved by all authors and tacitly or explicitly by the responsible authorities where the work was carried out.

Authors of the selected papers have to send the final camera ready paper (both in MS Word &PDF) for final print

After the review process, the selected papers will be published in the Journal.

Article structure

Subdivision - numbered sections

Divide your article into clearly defined and numbered sections. Subsections should be numbered 1.1 (then 1.1.1, 1.1.2, ...), 1.2, etc. (the abstract is not included in section numbering). Use this numbering also for internal cross-referencing: do not just refer to ‘the text’. Any subsection may be given a brief heading. Each heading should appear on its own separate line.

Introduction

State the objectives of the work and provide an adequate background, avoiding a detailed literature survey or a summary of the results.

Material and methods

Provide sufficient detail to allow the work to be reproduced. Methods already published should be indicated by a reference: only relevant modifications should be described.

Theory/calculation

A Theory section should extend, not repeat, the background to the article already dealt with in the Introduction and lay the foundation for further work. In contrast, a calculation section represents a practical development from a theoretical basis.

Results

Results should be clear and concise.

Discussion

This should explore the significance of the results of the work, not repeat them. A combined Results and Discussion section is often appropriate. Avoid extensive citations and discussion of published literature.

Conclusion

The main conclusions of the study may be presented in a short Conclusions section, which may stand alone or form a subsection of a Discussion or Results and Discussion section.

Appendices

If there is more than one appendix, they should be identified as A, B, etc. Formulae and equations in appendices should be given separate numbering: Eq. (A.1), Eq. (A.2), etc.; in a subsequent appendix, Eq. (B.1) and so on. Similarly for tables and figures: Table A.1; Fig. A.s1, etc.

NMAM INSTITUTE OF TECHNOLOGY, NITTE – 574110

NMAM Institute of Technology was started in the year 1986, as a part of Nitte Education Trust, Mangalore and is celebrated its Silver Jubilee in 2011. The Institute is named in fond memory of Nitte Mahalinga Adyanthaya, a distinguished engineer of the district. It is affiliated to the Visvesvaraya Technological University, Belgaum, enjoying academic autonomy and is recognized by the All India Council for Technical Education, New Delhi. It is accredited by the National Board for Accreditation and is certified to the ISO 9001 – 2008 standards for quality education by KEMA, Netherlands. The Institute has been recognized as Lead Institute under TEQIP- I Project of World Bank.

The Institute offers B.E, M.Tech and Ph.D pragrammes in various Engineering and Technology disciplines. The graduate programs comprise of 7 branches of Engineering – Electronics & Communication Engineering, Computer Science & Engineeing, Civil Engineering, Electrical & Electronics Engineering, Information Science & Engineering, Bio-Technology and Mechanical Engineering. The Institute's postgraduate programs include, Master of Technology in five disciplines, Master of Computer Applications and Master of Business Administration. The Visvesvaraya Technological University has opened a postgraduate extension centre at NMAMIT, offering M.Tech in Micro-electronics & Control Systems. Besides these, students also pursue their M.Sc(Eng.) and Doctoral Programs at the Institute. The Institute got academic autonomy in the year 2007, bringing in the much needed flexibility to innovate in terms of curriculum, education delivery and evaluation. Institute entered into collaboration with Penn State University, Harrisburg, USA and started offering 2+2 twinning program in Engineering since 2011.